

RESEARCH ARTICLE

A Sir2-regulated locus control region in the recombination enhancer of *Saccharomyces cerevisiae* specifies chromosome III structure

Mingguang Li¹ , Ryan D. Fine² , Manikarna Dinda², Stefan Bekiranov² , Jeffrey S. Smith¹ ^{2*}

1 Department of Laboratory Medicine, Jilin Medical University, Jilin, China, **2** Department of Biochemistry and Molecular Genetics, University of Virginia School of Medicine, Charlottesville, Virginia, United States of America

 These authors contributed equally to this work.

* jss5y@virginia.edu



 OPEN ACCESS

Citation: Li M, Fine RD, Dinda M, Bekiranov S, Smith JS (2019) A Sir2-regulated locus control region in the recombination enhancer of *Saccharomyces cerevisiae* specifies chromosome III structure. PLoS Genet 15(8): e1008339. <https://doi.org/10.1371/journal.pgen.1008339>

Editor: Kerstin Bystricky, Université de Toulouse-CNRS, FRANCE

Received: January 25, 2019

Accepted: August 1, 2019

Published: August 28, 2019

Copyright: © 2019 Li et al. This is an open access article distributed under the terms of the [Creative Commons Attribution License](https://creativecommons.org/licenses/by/4.0/), which permits unrestricted use, distribution, and reproduction in any medium, provided the original author and source are credited.

Data Availability Statement: Raw ChIP-seq and Hi-C sequencing data are available from the NCBI GEO database, accession# GSE92717. All other relevant data are within the manuscript and its Supporting Information files.

Funding: This work was supported by National Institutes of Health (<https://www.nih.gov/>) grants GM075240 and GM127394 to J.S.S. and GM110380 to S.B. National Institutes of Health training grant T32GM008136 provided partial support for R.D.F. Research startup grant

Abstract

The NAD⁺-dependent histone deacetylase Sir2 was originally identified in *Saccharomyces cerevisiae* as a silencing factor for *HML* and *HMR*, the heterochromatic cassettes utilized as donor templates during mating-type switching. *MATa* cells preferentially switch to *MATa* using *HML* as the donor, which is driven by an adjacent *cis*-acting element called the recombination enhancer (RE). In this study we demonstrate that Sir2 and the condensin complex are recruited to the RE exclusively in *MATa* cells, specifically to the promoter of a small gene within the right half of the RE known as *RDT1*. We also provide evidence that the *RDT1* promoter functions as a locus control region (LCR) that regulates both transcription and long-range chromatin interactions. Sir2 represses *RDT1* transcription until it is removed from the promoter in response to a dsDNA break at the *MAT* locus induced by HO endonuclease during mating-type switching. Condensin is also recruited to the *RDT1* promoter and is displaced upon HO induction, but does not significantly repress *RDT1* transcription. Instead condensin appears to promote mating-type donor preference by maintaining proper chromosome III architecture, which is defined by the interaction of *HML* with the right arm of chromosome III, including *MATa* and *HMR*. Remarkably, eliminating Sir2 and condensin recruitment to the *RDT1* promoter disrupts this structure and reveals an aberrant interaction between *MATa* and *HMR*, consistent with the partially defective donor preference for this mutant. Global condensin subunit depletion also impairs mating-type switching efficiency and donor preference, suggesting that modulation of chromosome architecture plays a significant role in controlling mating-type switching, thus providing a novel model for dissecting condensin function *in vivo*.

Author summary

Sir2 is a highly conserved NAD⁺-dependent protein deacetylase and defining member of the sirtuin protein family. It was identified 40 years ago in the budding yeast,

(2017kyqd001) from Jilin Medical University and a Jilin Provincial Department of Education, "13th five-Year" scientific and technological research project (JJKH20191056KJ) also provided support for M. L. The authors have no conflicts of interest. The funders had no role in study design, data collection and analysis, decision to publish, or preparation of the manuscript.

Competing interests: The authors have declared that no competing interests exist.

Saccharomyces cerevisiae, as a factor that silences the cryptic mating-type loci, *HML* and *HMR*. These heterochromatic cassettes are utilized as templates for mating-type switching, whereby a programmed DNA double-strand break at the *MATa* or *MAT α* locus is repaired by gene conversion to the opposite mating-type. This directional switching is called donor preference, which in *MATa* cells, is driven by a cis-acting DNA element called the recombination enhancer (RE). It was believed the only role for Sir2 in mating-type switching was silencing *HML* and *HMR*. However, we now show that Sir2 also regulates expression of a small gene (*RDT1*) in the RE that is activated during mating-type switching. The promoter of this gene is also bound by the condensin complex, and deleting this region of the RE drastically changes chromosome III structure and alters donor preference. The RE therefore appears to function as a complex locus control region (LCR) that links transcriptional control to chromatin architecture, thus providing a new model to investigate the underlying mechanistic principles of programmed chromosome architectural dynamics.

Introduction

Since the first descriptions of mating-type switching in budding yeast over 40 years ago, characterization of this process has led to numerous advances in understanding mechanisms of gene silencing (heterochromatin), cell-fate determination (mating-type), and homologous recombination (reviewed in [1]). For example, the NAD⁺-dependent histone deacetylase, Sir2, and other Silent Information Regulator (SIR) proteins, were genetically identified due to their roles in silencing the heterochromatic *HML* and *HMR* loci, which are maintained as silenced copies of the active *MAT α* and *MATa* loci, respectively [2–4]. The SIR silencing complex (Sir2-Sir3-Sir4) is recruited to cis-acting E and I silencer elements flanking *HML* and *HMR* through physical interactions with silencer binding factors Rap1, ORC, and Abf1, as well as histones H3 and H4 (reviewed in [5]).

HML and *HMR* play a critical role in mating-type switching. Haploid cells of the same mating-type cannot mate to form diploids, the preferred cell type in the wild. Therefore, in order to facilitate mating and diploid formation, haploid mother cells switch their mating-type by expressing HO endonuclease, which introduces a programmed DNA double-strand break (DSB) at the *MAT* locus [6]. The break is then repaired by homologous recombination using either *HML* or *HMR* as a donor template for gene conversion [6, 7]. This change in mating-type enables immediate diploid formation between mother and daughter. *HO* is deleted from most standard lab strains in order to maintain them as haploids, so expression of *HO* from an inducible promoter such as P_{GALI} is commonly used to switch mating-types during strain construction [8].

There is a “donor preference” directionality to mating-type switching such that ~90% of the time, the HO-induced DSB is repaired to the opposite mating-type [9]. For example, *MAT α* cells preferentially switch to *MATa* using *HMR* as the donor. However, while both silent mating loci can be utilized as a donor template, usage of *HML* by *MATa* cells requires a 2.5 kb intergenic region located ~17 kb from *HML* called the recombination enhancer (RE) [10]. Donor preference activity within the RE has been further narrowed down to a 700 bp segment containing an Mcm1/ α 2 binding site (DPS1) and multiple Fkh1 binding sites [10]. The RE is active in *MATa* cells, requiring Mcm1 and Fkh1 activity at their respective binding sites [10–12]. The RE is inactivated in *MAT α* cells due to expression of transcription factor α 2 from *MAT α* [13], which forms a repressive heterodimer with Mcm1 (Mcm1/ α 2) to repress *MATa*-

specific genes [1]. Current models for donor preference posit that Fkh1 at the RE helps position *HML* in close proximity with *MATa* by interacting with threonine-phosphorylated H2A (γ -H2AX) and Mph1 DNA helicase at the HO-induced DNA DSB [14, 15].

Sir2-dependent silencing of *HML* and *HMR* has two known functions related to mating-type switching. First, *HML* and *HMR* must be silenced in haploids to prevent formation of the $\alpha 1/\alpha 2$ heterodimer, which would otherwise inactivate haploid-specific genes such as *HO* [16]. Second, heterochromatin structure at *HML* and *HMR* blocks cleavage by HO, thus restricting its activity to the fully accessible *MAT* locus [17, 18]. Here we describe new roles for Sir2 and the condensin complex within the RE during mating-type switching. ChIP-seq analysis revealed strong overlapping binding sites for Sir2 and condensin at the promoter of a small gene within the RE known as *RDT1*. Here, Sir2 was found to repress the *MATa*-specific transcription of *RDT1*, which is also translated into a small 28 amino acid peptide. *RDT1* expression is also dramatically upregulated during mating-type switching when Sir2 is lost from the *RDT1* promoter and instead associates with the HO-induced DNA DSB at *MATa*. Furthermore, eliminating Sir2/condensin recruitment to the *RDT1* promoter disrupts chromosome III architecture such that donor preference is partially impaired. The *RDT1* promoter region therefore functions like a classic locus control region (LCR) in *MATa* yeast cells, regulating localized transcription as well as long-range chromosome interactions.

Results

Sir2 and condensin associate with the recombination enhancer (RE)

We previously characterized global sirtuin distribution using ChIP-Seq to identify novel loci regulated by Sir2 and its homologs [19]. Significant overlap was observed between binding sites for Sir2, Hst1, or Sum1 with previously described condensin binding sites [19, 20], suggesting a possible functional connection. ChIP-Seq was therefore performed on WT and *sir2* Δ strains in which the condensin subunit Smc4 was C-terminally tagged (13xMyc) (Fig 1A). To avoid “hyper-ChIPable” loci that can appear in yeast ChIP-seq experiments, we also ran nuclear localized GFP controls [21]. Genes closest to Sir2-dependent condensin peaks after subtraction of GFP are listed in S1 Table, and are distributed throughout the genome. One of the strongest peaks overlapped with a Sir2-myc binding site on chromosome III between *KAR4* and *SPB1* that was not enriched for GFP (Fig 1A). The specificity of Sir2 enrichment at this peak, as opposed to the adjacent *SPB1* gene, was independently confirmed by quantitative ChIP using an α -Sir2 antibody (Fig 1B), with enrichment comparable to levels observed at the *HML-I* silencer (Fig 1A and 1B). Sir2-dependent condensin binding was also confirmed for Myc-tagged Smc4 and Brn1 subunits (Fig 1C). The ~2.5 kb intergenic region between *KAR4* and *SPB1* was previously defined as a cis-acting recombination enhancer (RE) that specifies donor preference of mating-type switching in *MATa* cells [10, 13]. Quantitative ChIP assays revealed that Sir2 and Brn1-myc enrichment at the RE was also *MATa*-specific (Fig 1D and 1E), which was notable because the ChIP-seq datasets in Fig 1A happened to be generated from *MATa* strains. We next considered whether the condensin binding defect in the *MATa* *sir2* Δ mutant was due to *HMLALPHA2* expression caused by defective *HML* silencing. To test this idea, we re-examined Brn1-myc ChIP signal at the RE in strains lacking *HML*, and found that deleting *SIR2* no longer affected condensin recruitment (Fig 1F). Similarly, a *MATa* condensin mutant (*ycs4-1*) known to have an *HML* silencing defect [22] reduced Sir2 recruitment to the RE, but had no effect when *HML* was also deleted (Fig 1G). Sir2 and condensin are therefore independently recruited to the RE only in *MATa* cells.

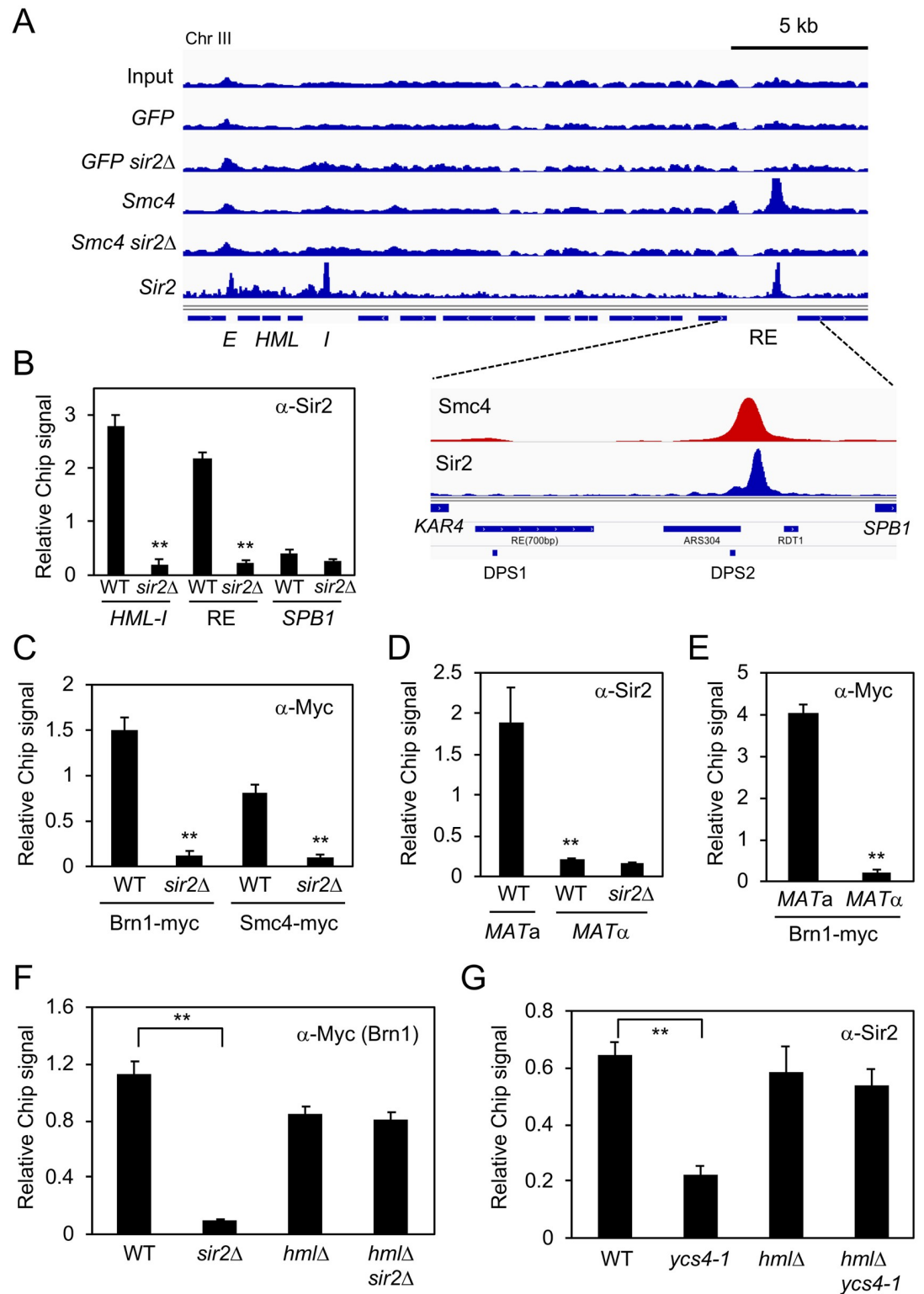


Fig 1. *MATa*-specific binding of Sir2 and condensin to the recombination enhancer (RE). (A) ChIP-seq of *Smc4*-myc, *Sir2*-myc, and nuclear localized GFP in WT and *sir2*Δ backgrounds. The left arm of chromosome III is depicted from *HML* to *SPB1*. RE indicates the recombination enhancer region. Inset: The minimal 700bp RE element required for donor preference is indicated, as are the two *Mcm1/α2* binding sites (*DPS1* and *DPS2*) and *RDT1*. (B) *Sir2* ChIP at the RE, *HML-I* silencer, and *SPB1*. (C) α-Myc ChIP of *Brn1*-myc and *Smc4*-myc at the RE. (D) ChIP showing *MATa*-specific binding of *Sir2* to the RE. (E) α-Myc ChIP of *Brn1*-myc at the RE. (F) α-Myc ChIP of *Brn1*-myc at the RE. (G) α-Sir2 ChIP at the RE in WT, *ycs4-1*, *hml*Δ, and *hml*Δ *ycs4-1* backgrounds.

(E) ChIP showing *MATa*-specific binding of Brn1-myc to the RE. (F) Brn1-Myc ChIP at RE is not Sir2 dependent. (G) Native Sir2 ChIP at RE is not condensin dependent. The ChIP signal in each panel is relative to input and plotted as the mean of three replicates. Error bars = standard deviation. (** $p < 0.005$).

<https://doi.org/10.1371/journal.pgen.1008339.g001>

Sir2 regulates a small gene (*RDT1*) within the RE

Donor preference activity ascribed to the RE was previously narrowed down to a *KAR4* (*YCL055W*)-proximal 700 bp domain defined by an *Mcm1/α2* binding site (Fig 2A, *DPS1*) [10, 11, 13]. The Sir2 and condensin ChIP-seq peaks we identified were located outside this region, between a second *Mcm1/α2* binding site (*DPS2*) and a small gene of unknown function called *RDT1* [23] (Figs 1A and 2A). We noticed the location of *RDT1* coincided with the smallest of several putative non-coding RNAs (ncRNA) previously reported as being transcribed from the RE, but not annotated in SGD (Fig 2A, [13]). Quantitative RT-PCR and analysis of publicly available RNA-seq data from BY4741 (*MATa*) and BY4742 (*MATα*) revealed that *RDT1* expression was indeed *MATa* specific (Fig 2B and S1A Fig).

We next asked whether Sir2 and/or condensin regulate histone acetylation and *RDT1* expression when recruited to the RE. Sir2 normally represses transcription at *HML*, *HMR*, and telomeres as a catalytic subunit of the SIR complex where it preferentially deacetylates H4K16 (reviewed in [5]). Accordingly, deleting *SIR2*, *SIR3*, or *SIR4* from *MATa* cells increased H4K16 acetylation at the *RDT1* promoter (Fig 2C), consistent with the observed enrichment of Sir3-myc and Sir4-myc at this site (S1B Fig). Furthermore, re-introducing active *SIR2* into the *sir2Δ* mutant restored H4K16 to the hypoacetylated state, whereas catalytically inactive *sir2-H364Y* did not (Fig 2D). While H4K16ac is a preferred Sir2 substrate for silencing at *HML* and *HMR*, the recruited SIR complex also maintains lysine deacetylation of the other N-terminal histone tails [24]. Since *RDT1* transcription is *MATa* specific, and *Mcm1/α2* represses *MATa*-specific genes by recruiting the Ssn6/Tup1 corepressor complex and Class I/II HDACs such as the H3/H2B-specific histone deacetylase HDA1 [25, 26], we also tested the effect of deleting *SIR2* on H3K9/14 acetylation at the *RDT1* promoter, predicting it may remain hypoacetylated due to the SIR complex being replaced by Ssn6/Tup1/HDA1. Indeed, H3K9/14 acetylation was reduced in the *sir2Δ* mutant relative to WT, but was significantly elevated in the *hmlΔ sir2Δ* double mutant (Fig 2E). *RDT1* expression was similarly reduced in the *sir2Δ* mutant and strongly upregulated when *HML* and *SIR2* were both deleted (Fig 2F). An even stronger expression effect was observed in an *hmlΔ sir2Δ hst1Δ* triple mutant that eliminates any possibility of redundancy between the Sir2 and Hst1 paralogs (S1C Fig). On the other hand, *RDT1* was not upregulated in an *hmlΔ ycs4-1* condensin mutant (Fig 2G). Taken together, these results provide strong evidence that the SIR complex represses *RDT1* in *MATa* cells by establishing a generally hypoacetylated chromatin environment at the promoter, while condensin has a functional role independent of transcriptional regulation.

We next attempted to prevent Sir2 and condensin recruitment to the *RDT1* promoter by precisely deleting a 100bp DNA sequence underlying the shared enrichment region (coordinates 30701–30800), while not disturbing the adjacent *Mcm1/α2* site (Fig 3A). Sir2 and Brn1-myc binding to the RE as measured by ChIP was greatly diminished in this mutant (Fig 3B and 3C), despite unaltered Sir2, Brn1-myc, or Smc4-myc expression levels (S2A–S2C Fig). Furthermore, *RDT1* RNA expression level was significantly increased by the 100bp deletion exclusively in *MATa* cells (Fig 3D), consistent with the loss of Sir2-mediated repression.

Because Sir2 and condensin were not present at the *RDT1* promoter in *MATα* cells, we reasoned that their binding should require a *MATa* specific transcription factor. This made the 2nd *Mcm1/α2* binding site (*DPS2*) upstream of the Sir2/condensin ChIP-seq peaks an ideal

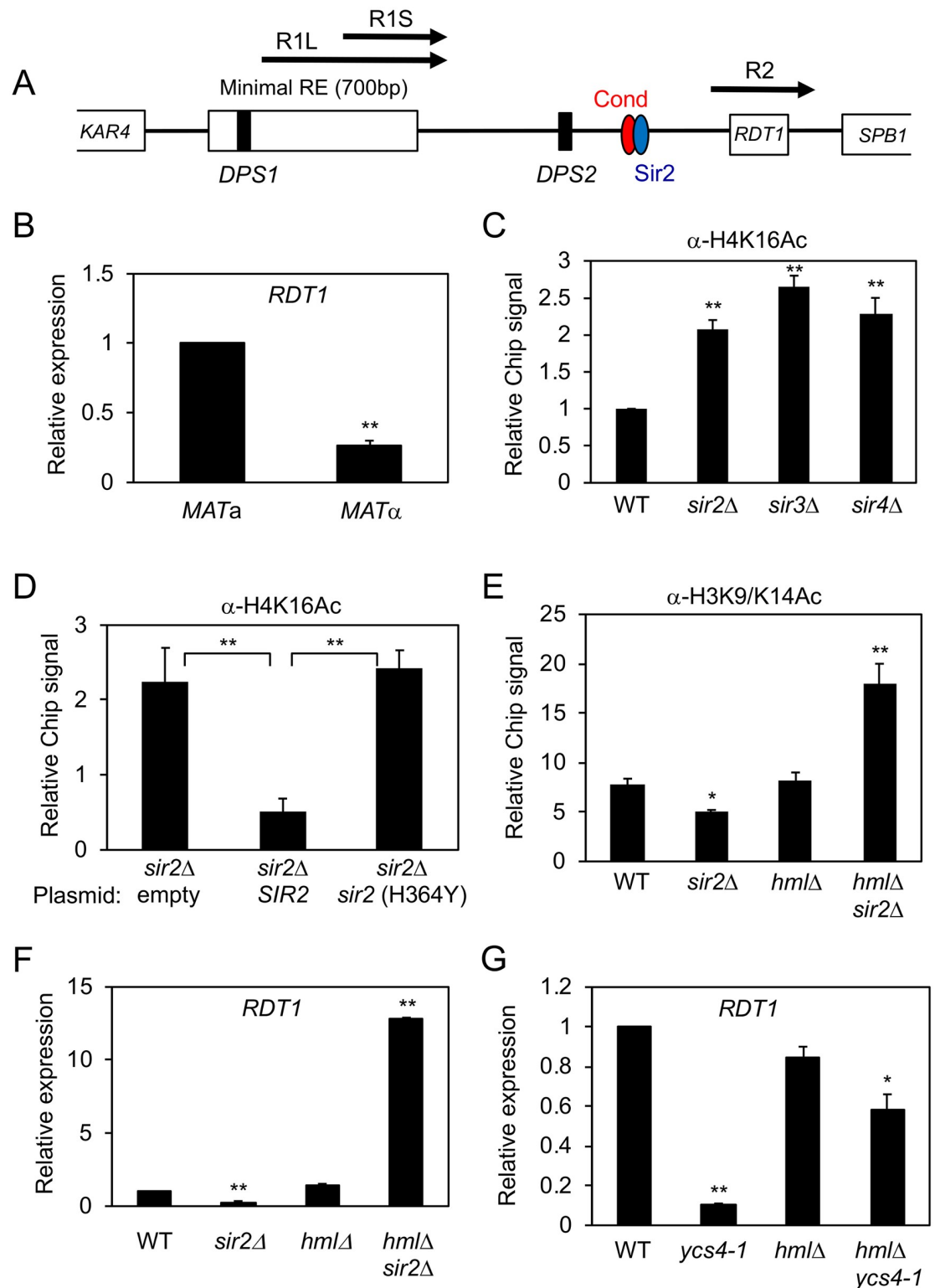


Fig 2. *RDT1* is a novel Sir2 regulated gene. (A) Schematic of the RE locus depicting Sir2/Condensin peak locations relative to previously reported R1L/S and R2 (*RDT1*) RNAs. (B) *RDT1* mRNA expression is *MATa* specific. *RDT1* expression level is calculated relative to the *ACT1* control. This *RDT1/ACT1* ratio is then normalized to 1.0 for the *MATa* strain. (C) H4K16ac ChIP signal at RE in SIR complex null strains, relative to input signal. WT is normalized to 1.0. (D) H4K16 deacetylation is dependent on Sir2 catalytic activity. A *sir2Δ* strain was transformed with the indicated plasmids and ChIP assays performed. ChIP signal is

relative to input. (E) Effect of *sir2Δ* on H3K9/K14ac ChIP at the *RDT1* promoter in *HML* and *hmlΔ* backgrounds. ChIP signal is relative to input. (F) Differential *RDT1* transcriptional regulation by *SIR2* is dependent on *HML* status. *RDT1* expression is relative to the *ACT1* control, and the *RDT1/ACT1* ratio is normalized to 1.0 for WT. (G) Effects of the *ycs4-1* mutation on *RDT1* expression in *HML* and *hmlΔ* backgrounds at 30°C. (* $p < 0.05$; ** $p < 0.005$). *RDT1* expression is plotted as for panel F.

<https://doi.org/10.1371/journal.pgen.1008339.g002>

candidate, because it had not previously been ascribed a function other than redundancy with DPS1 for donor preference [13]. Deleting *MCM1* is lethal, so alternatively, we precisely deleted the 2nd *Mcm1/α2* binding site (ChrIII coordinates 30595 to 30626, S3A Fig) and then retested for Sir2 and Brn1-myc enrichment. As shown in S3B and S3C Fig, respectively, Sir2 and Brn1-myc enrichment at the *Mcm1/α2* binding site (DPS2) and the *RDT1* promoter (defined as the Sir2/condensin peaks) was significantly reduced in the binding site mutant. These results suggest that *Mcm1* nucleates a complex that recruits the SIR and condensin complexes to the *RDT1* promoter in *MATα* cells, and also provides a possible mechanism of blocking the recruitment in *MATα* cells due to the interaction of *Mcm1* with *α2*.

***RDT1* encodes a translated mRNA**

Ribosome Detected Transcript-1 (*RDT1*) was originally annotated as a newly evolved gene whose transcript was associated with ribosomes and predicted to have a small open reading frame of 28 amino acids [23]. Our work suggested that *RDT1* and the putative non-coding R2 transcript were the same (Fig 2A). To determine if *RDT1/R2* codes for a small protein, the ORF was C-terminally fused with a 13x-Myc epitope in *MATα* and *MATa* cells. As shown in Fig 3E, a fusion protein was exclusively detected in exponentially growing *MATα* WT cells and also highly expressed in the 100bpΔ strain, correlating with the increased RNA level observed for that mutant in Fig 3D.

Since additional *MATα*-specific RNAs are derived from the minimal 700bp RE domain (Fig 2A; R1L and R1S) [13, 27], we next tested whether Sir2/condensin recruitment to the *RDT1* promoter had any effect on expression of these upstream ncRNAs from a distance. Quantitative RT-PCR for the R1L/S transcripts indicated their expression level in the WT strain was comparable to *RDT1*, and was also reduced in a *sir2Δ* mutant because of the pseudodiploid phenotype (Fig 3F). However, while *RDT1* was strongly upregulated by the 100bp deletion of the Sir2/condensin binding site, R1L/S expression was unaffected (Fig 3F). As a control, we also measured expression of the *SPB1* gene located immediately downstream of *RDT1* (see Fig 2A schematic). *SPB1* expression is not mating-type specific, it encodes a rRNA methyltransferase required for maturation of the large 60S ribosomal subunit [28], and interestingly, also functions in silencing at *HML* and *HMR* [29]. It was therefore intriguing that *SPB1* expression was increased 2- to 3-fold in the *sir2Δ* and 100bpΔ mutants (Fig 3G), suggesting that Sir2 at the *RDT1* promoter has a modest downstream repressive effect on *SPB1*, but not on the upstream R1L/S ncRNAs. Notably, steady state *RDT1* and R1L/S RNA levels were relatively low compared to *SPB1* and the *ACT1* loading control, even in the 100bpΔ mutant (Fig 3G).

Sir2 and condensin are displaced from the *RDT1* promoter during mating-type switching

We next asked if Sir2 played any role in regulating *RDT1* during mating-type switching. Sir2 was previously shown to associate with a HO-induced DSB at the *MAT* locus during mating-type switching, presumably to effect repair through histone deacetylation [30]. SIR complex association with DSBs occurs at the expense of telomere binding [31], so we hypothesized that the HO-induced DSB at *MAT* could also trigger loss of Sir2 from the *RDT1* promoter, thus facilitating increased *RDT1* transcription. To test this idea, HO was induced at time 0 with

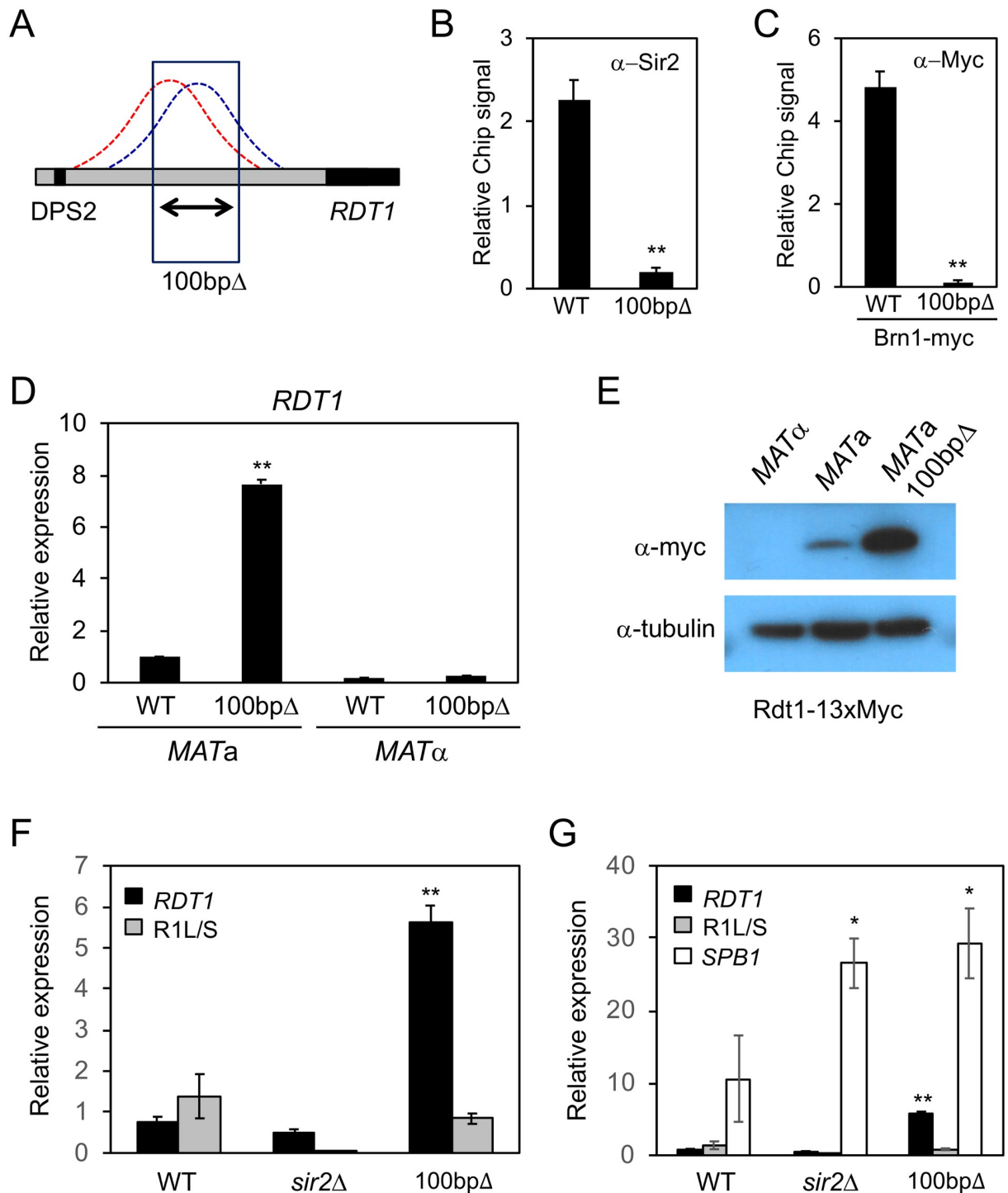


Fig 3. Identification of a 100bp sequence that recruits Sir2/condensin and represses *RDT1* expression. (A) Schematic indicating a 100bp deletion that covers the condensin (red) and Sir2 (blue) peaks. (B) ChIP of Sir2 in the 100bpΔ mutant (ML275). (C) ChIP of Brn1-Myc in the 100bpΔ mutant. ChIP PCR signal in panels B and C is plotted relative to the input signal. (D) *RDT1* transcription in *MATa* cells is derepressed in the 100bpΔ mutant. The *RDT1* level is plotted relative to *ACT1* control, and then normalized to 1.0 for the WT *MATa* strain. (E) Western blot of Rdt1-13xMyc in WT *MATα* and *MATa* cells, as well as the *MATa* 100bpΔ mutant. Predicted fusion protein molecular weight is 19.1 kDa, but it runs ~37 kDa. (F) Comparative *RDT1* and R1L/S expression levels in WT, *sir2Δ*, and 100bpΔ strains. One of the WT *RDT1* qPCR replicates was normalized to 1.0 to allow direct comparisons between *RDT1* and R1L/S levels. (G) Comparative *RDT1*, R1L/S, and *SPB1* expression levels in WT, *sir2Δ*, and 100bpΔ strains. As in panel F, one of the WT *RDT1* qPCR replicates was normalized to 1.0. (* $p < 0.05$; ** $p < 0.005$, compared to WT strain).

<https://doi.org/10.1371/journal.pgen.1008339.g003>

galactose and then turned off 2 hours later by glucose addition to allow for repair/switching to occur (Fig 4A and 4B). By the 3 hr time point (1 hr after glucose addition), ChIP analysis indicated Sir2 was maximally enriched at the *MAT* locus (Fig 4C), corresponding to the time of peak mating-type switching ([30] and Fig 4B). Interestingly, Sir2 was significantly depleted from the *RDT1* promoter within 1 hr after HO induction, and by 3 hr there was actually stronger enrichment of Sir2 at *MAT* than *RDT1* (Fig 4C). Critically, this shift in Sir2 distribution correlated with maximal induction of *RDT1* mRNA and the Myc-tagged Rdt1 protein (Fig 4D and 4E, 3 hr). Once switching was completed by 4 hr (2 hr after glucose addition), *RDT1* transcription was permanently inactivated and Sir2 binding never returned because most cells were now *MAT α* . The Myc-tagged Rdt1 protein, however, remained elevated for the rest of the time course (Fig 4E), suggesting that it is relatively stable, at least when epitope tagged. A parallel ChIP time course experiment was performed with condensin (Brn1-myc), indicating significant depletion from the *RDT1* promoter within 1 hr (Fig 4F), similar to the timing of Sir2 loss. Unlike Sir2, Brn1-myc enrichment at the HO-cleaved *MAT* site did not increase, suggesting that condensin normally associates with *MAT α* in non-switching cells and is then displaced in response to the HO-induced DSB, perhaps to facilitate structural reorganization associated with switching.

Since *RDT1* was highly expressed during mating-type switching, we next asked whether the small protein encoded by this gene had a direct function during the switching process when using the galactose-inducible system employed in this study. The 28 amino acid ORF was precisely deleted using the *delitto perfetto* method [32], and the efficiency of switching from *MAT α* to *MAT α* was then tested across a time course by PCR (S4A and S4B Fig). No significant differences were observed between the WT and *rdt1 Δ* strains. Next, donor preference was tested using a strain previously developed by the Haber lab [15], whereby *HMR α* was replaced with *HMR α* containing a unique *Bam*HI site (*HMR α -B*) (S4C Fig). Following completion of Gal-HO-induced switching from *MAT α* to *MAT α* , the proportion of donor utilization was determined by *Bam*HI digest of a *MAT α* PCR product. As shown in S4D and S4E Fig, deleting *RDT1* also had no effect on donor preference, indicated by low utilization (~9%) of *HMR α -B*. Therefore, although *RDT1* gene expression strongly correlates with switching, a specific function for its gene product remains elusive. Therefore, we shifted our attention to a possible function for the *RDT1* promoter.

The *RDT1* promoter region controls chromosome III architecture

The coupling of Sir2 and condensin distribution with *RDT1* transcriptional regulation during mating-type switching was reminiscent of classic locus control regions (LCR) that modulate long-range chromatin interactions [33, 34]. We therefore hypothesized that the *RDT1* promoter region functions as an LCR to modulate long-range chromatin interactions of chromosome III. To test this hypothesis, we performed Hi-C analysis with WT, *sir2 Δ* and the 100bp Δ strains. Genomic contact differences between the mutants and WT were quantified using the HOMER Hi-C software suite [35], and the frequency of statistically significant differences for each chromosome calculated (Fig 5A). Chromosome III had the most significant differences in both mutants, so we focused on this chromosome and used HOMER to plot the observed/expected interaction frequency in 10kb bins for each strain as a heat map (Fig 5B). In a WT strain (ML1) there was strong interaction between the left and right ends of chromosome III, mostly centered around the *HML* (bin 2) and *HMR* (bin 29) loci. Interestingly, *HML* (bin 2) also appeared to sample the entire right arm of chromosome III, with the interaction frequency increasing as a gradient from *CEN3* to a maximal observed interaction at *HMR*, thus also encompassing the *MAT α* locus at bin 20. This distinct interaction pattern was completely

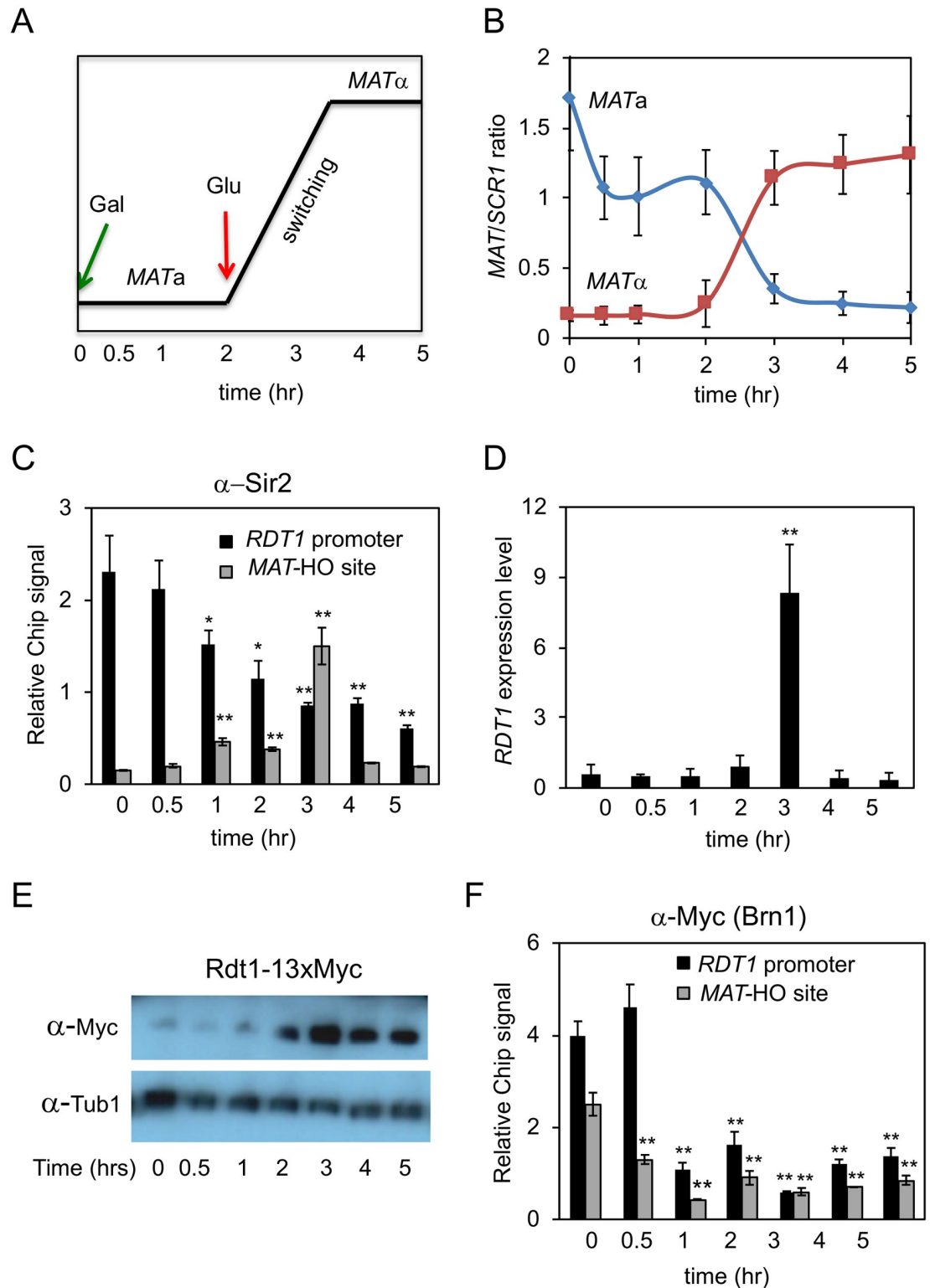


Fig 4. Dynamics of Sir2 and condensin binding at the *RDT1* promoter and *MATa* locus during mating-type switching. (A, B) Quantitation of a mating-type switching time course where HO was induced by galactose at time 0, then glucose added at 2 hr to stop HO expression and allow for break repair. Switching is maximal at 3 hr. The average ratios of *MATa* and *MATα* PCR products relative to an *SCR1* loading control PCR product were plotted (n = 3 biological replicates). (C) ChIP of Sir2 at the *RDT1* promoter and the HO-induced DSB site (*MAT-HO*). (D) qRT-PCR of *RDT1* expression relative to *ACT1* across the mating-type

switching time course. The time 0 level is normalized to 1. (E) Rdt1-13xMyc protein expression across the same time course. (F) ChIP of Brn1-myc at the *RDT1* promoter and *MAT*-HO break site across the same time course. ChIP signal PCR is plotted relative to the input signal. (* $p < 0.05$, ** $p < 0.005$ compared to time 0).

<https://doi.org/10.1371/journal.pgen.1008339.g004>

disrupted in the *sir2Δ* mutant, whereas some telomere-subtelomere contacts were retained in the 100bpΔ mutant (Fig 5B), suggesting there was still limited interaction between the left and right ends of the chromosome. We confirmed the changes in *HML*-*HMR* interaction for these strains using a quantitative 3C-PCR assay to rule out sequencing artifacts (Fig 5C), and to confirm an earlier *sir2Δ* 3C result from the Dekker lab [36]. Importantly, despite the loss of *HML*-*HMR* interaction in the 100bpΔ mutant, heterochromatin at these domains was unaffected based on normal quantitative mating assays (S5A Fig), and unaltered Sir2 association with *HML* (S5B Fig).

We next analyzed the Hi-C data using an iterative correction method that reduces background to reveal interacting loci that potentially drive the overall chromosomal architecture, rather than passenger locus effects [37]. *HML* (bin 2) and *HMR* (bin 29) again formed the dominant interaction pair off the diagonal in WT, which was lost in the *sir2Δ* or 100bpΔ mutants (Fig 5D, red arrows). Importantly, a prominent new interaction between *HMR* (bin 29) and *MATa* (bin 20) appeared in both mutants (Fig 5D, black arrows), as would be predicted if normal donor preference of *MATa* cells was altered. We conclude that the *RDT1* promoter does function like an LCR in *MATa* yeast cells, regulating localized transcription and establishing a long-range chromatin interaction between *HML* and *HMR* that appears to prevent *HMR* from strongly associating with *MATa* (Fig 5E).

Sir2 and condensin regulate mating-type switching

Sir2/condensin binding was observed in the right half of the RE (Fig 1A), but this region was previously reported as dispensable for donor preference activity [10]. Considering that *HMR* was aberrantly associated with the *MATa* locus in *sir2Δ* and 100bpΔ mutants (Fig 5B–5E), we proceeded to test whether these mutants had any alterations in donor preference. As was done for the *rdt1Δ* mutant in S4C and S4D Fig, the 100bpΔ mutation was introduced into a reporter strain with *HMRα-B* on the right arm of chromosome III (Fig 6A; [15]). After inducing switching to *MATα* with galactose, the proportion of *HMLα* or *HMRα-B* used for the switching was determined by *Bam*HI digestion of a *MATα*-specific PCR product (Fig 6B; [15]). As expected for normal donor preference, *HMRα-B* on the right arm was only utilized ~9% of the time in the WT strain (Fig 6C and 6D). Strikingly, donor preference was lost in the *sir2Δ* mutant, similar to a control strain with the RE deleted (Fig 6C and 6D), and consistent with the clear interaction between *HMR* and *MATa* bins observed for the *sir2Δ* mutant in Fig 5D and 5E. This interaction was less prominent in the 100bpΔ mutant (Fig 5D), and the corresponding donor preference defect was also less severe (~25% *HMRα-B*), though still significantly different from WT (Fig 6C and 6D).

Since the donor preference assay is an endpoint experiment, we next tested whether the *sir2Δ* or 100bpΔ mutations temporally impacted the efficiency of switching from *MATa* to *MATα* in the same ML1 background strains used for Hi-C analysis. As shown in Fig 6E and 6F, switching efficiency was dramatically impaired in the *sir2Δ* strain, but unaffected in the 100bpΔ mutant. These results suggest a model whereby condensin and Sir2 recruitment to the *RDT1* promoter supports donor preference by organizing chromosome III into a structure that limits *HMR* association with the *MATa* locus, but is not required for the mechanics of mating-type switching. We suspect at least part of the strong *sir2Δ* effect on chromosome III organization and donor preference is caused by *HMLALPHA2* derepression, which inactivates

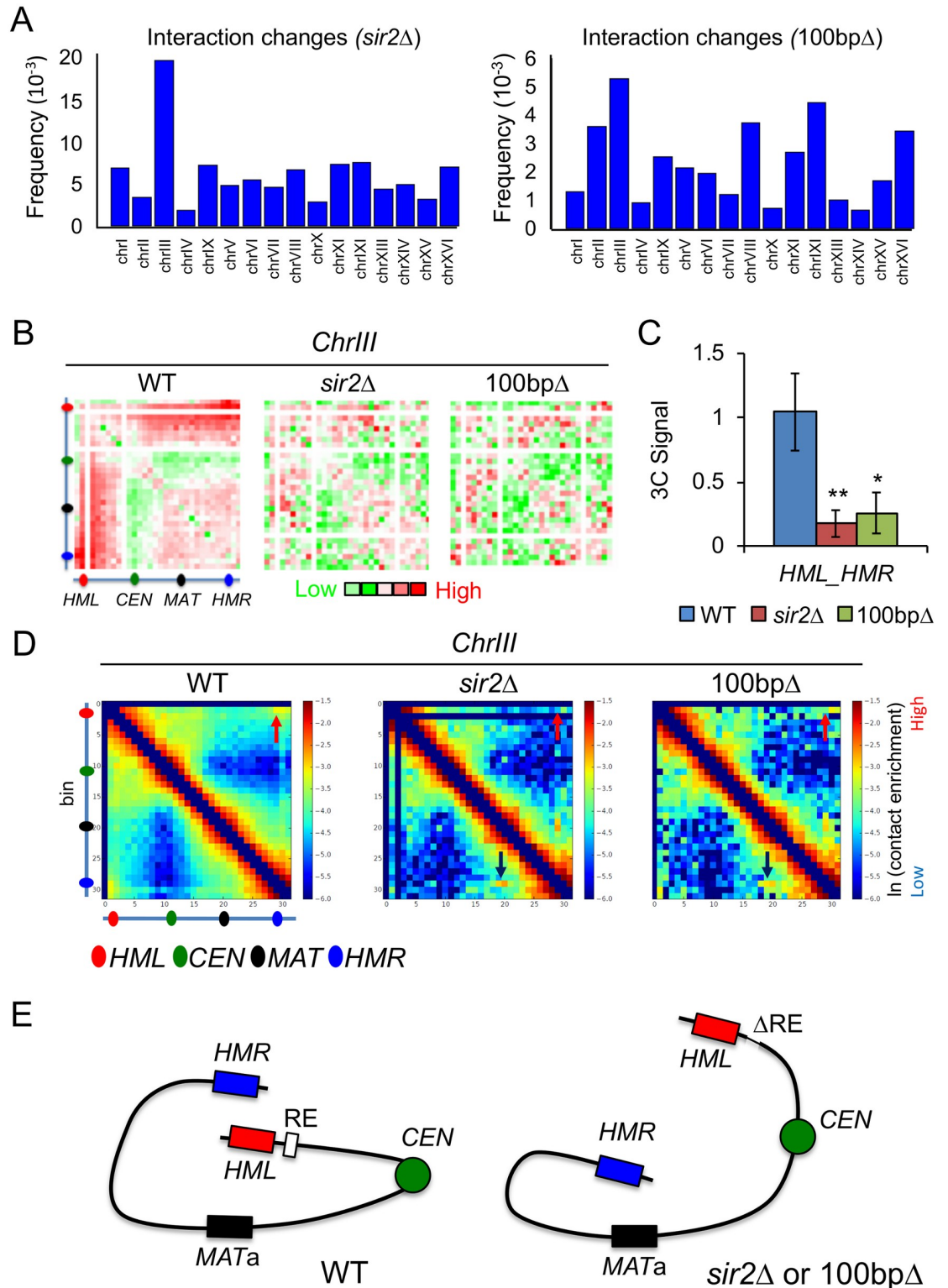


Fig 5. The Sir2/condensin binding site controls chromosome III architecture. (A) Frequency of significant Hi-C interaction changes identified using HOMER for each chromosome in the *sir2Δ* (ML25) and 100bpΔ (ML275) strains compared to WT (ML1). (B) HOMER-generated log₂ observed/expected Hi-C interaction frequency heat maps (10kb bins) for chromosome III. Solid white lines indicate bins with insufficient read coverage post-filtering. (C) qPCR detection of HML-HMR interaction using 3C analysis, with the WT signal normalized to 1. (*p < 0.05, ** < 0.005). (D) Iteratively corrected and read-normalized Hi-C heat maps

revealing an interaction between *HMR* (bin 29) and *MATa* (bin 20) in the *sir2Δ* and 100bpΔ mutants (black arrow). Solid black lines indicate bins with insufficient read coverage post-filtering. Red arrows indicate the *HML-HMR* interaction. (E) Summary of large-scale changes in chromosome III architecture. Δ indicates the 100bp deletion.

<https://doi.org/10.1371/journal.pgen.1008339.g005>

the RE due to formation of the Mcm1/α2 heterodimer [13]. We also considered a possibility that the *sir2Δ* heterochromatin defect at *HML* and *HMR* could make them highly accessible to HO cleavage [38], which would prevent their usage as donor templates. As a measure of HO cleavage at *MATa*, *HML*, or *HMR*, we assayed for reduced PCR amplification across the recognition site following Gal-HO induction (S6 Fig). While *MATa* was equally cut by HO in WT and *sir2Δ* strains (S6A and S6B Fig), *HML* was only cut in the *sir2Δ* strain (S6A and S6C Fig), consistent with the idea of reduced *HML* availability for switching. Unexpectedly, *HMR* remained available as a template in the *sir2Δ* strain (S6A and S6D Fig). We confirmed the difference in HO accessibility between *HML* and *HMR* using real-time qPCR (S6E and S6F Fig), which could contribute to the extreme *sir2Δ* donor preference defect (Fig 6C and 6D). In the 100bpΔ mutant, which locally eliminates condensin recruitment at *RDT1*, the continued maintenance of heterochromatin at *HML/HMR* and telomeres (S5 Fig), as well as residual telomere clustering (Fig 5D), may partially buffer the resulting donor preference defect by still limiting contact between the subtelomeric *HMR* locus and *MATa*.

Condensin recruitment to the *RDT1* promoter does not appear critical for the mechanics of mating-type switching, as indicated by normal timing of switching in the 100bpΔ mutant (Fig 6E and 6F). However, condensin could still potentially impact the switching process independent of the RE. In order to test this hypothesis, we C-terminally tagged the Brn1 condensin subunit with an auxin-inducible degron (AID) fused with a V5 epitope, which allows for rapid depletion of tagged proteins upon the addition of auxin [39]. Indeed, Brn1-AID was effectively degraded within 15 min of adding auxin to cells, as measured by western blotting (S7A Fig), or ChIP at the *RDT1* promoter (S7B Fig). Importantly, even after 1 hr of auxin treatment, there were no significant changes in *RDT1* or *HMLALPHA2* gene expression as measured by qRT-PCR (S7C and S7D Fig), thus indicating that silencing of *HML* was unaffected, unlike the *ycs4-1* condensin mutant used in Fig 1G [22]. The efficiency of ML1 switching from *MATa* to *MATα* was then tested across a time course with or without auxin treatment (Fig 7A). As shown in Fig 7B and 7C, auxin significantly slowed the efficiency of switching to *MATα*, indicating that the Brn1 subunit of condensin is important for normal mating-type switching.

Since the 100bpΔ mutant caused a modest donor preference defect that we partially attributed to a loss of condensin (Fig 6C and 6D), it was important to also test for a donor preference defect when condensin was depleted. Indeed, Brn1-AID depletion produced a significant defect in donor preference using the *HMRα-B* reporter strain (Fig 7D) that was similar in magnitude to that observed for the 100bpΔ strain (Fig 6D). Taken together, these results support a working model whereby condensin recruitment to the *RDT1* promoter in *MATa* cells organizes chromosome III into a conformation that limits the association of *HMR* with *MATa*, thus partially contributing to donor preference regulation. We hypothesize that upon HO cleavage of *MATa*, the increased expression of *RDT1* caused by loss of Sir2, displaces condensin from the promoter, which then allows the left half of the RE to physically direct *HML* to *MATa* for use as a donor (Fig 8).

Discussion

SIR2 was identified ~40 years ago as a recessive mutation unlinked from *HML* and *HMR* that caused their derepression [3, 4], and has been extensively studied ever since as encoding a heterochromatin factor that functions not only at the *HM* loci, but also telomeres and the rDNA

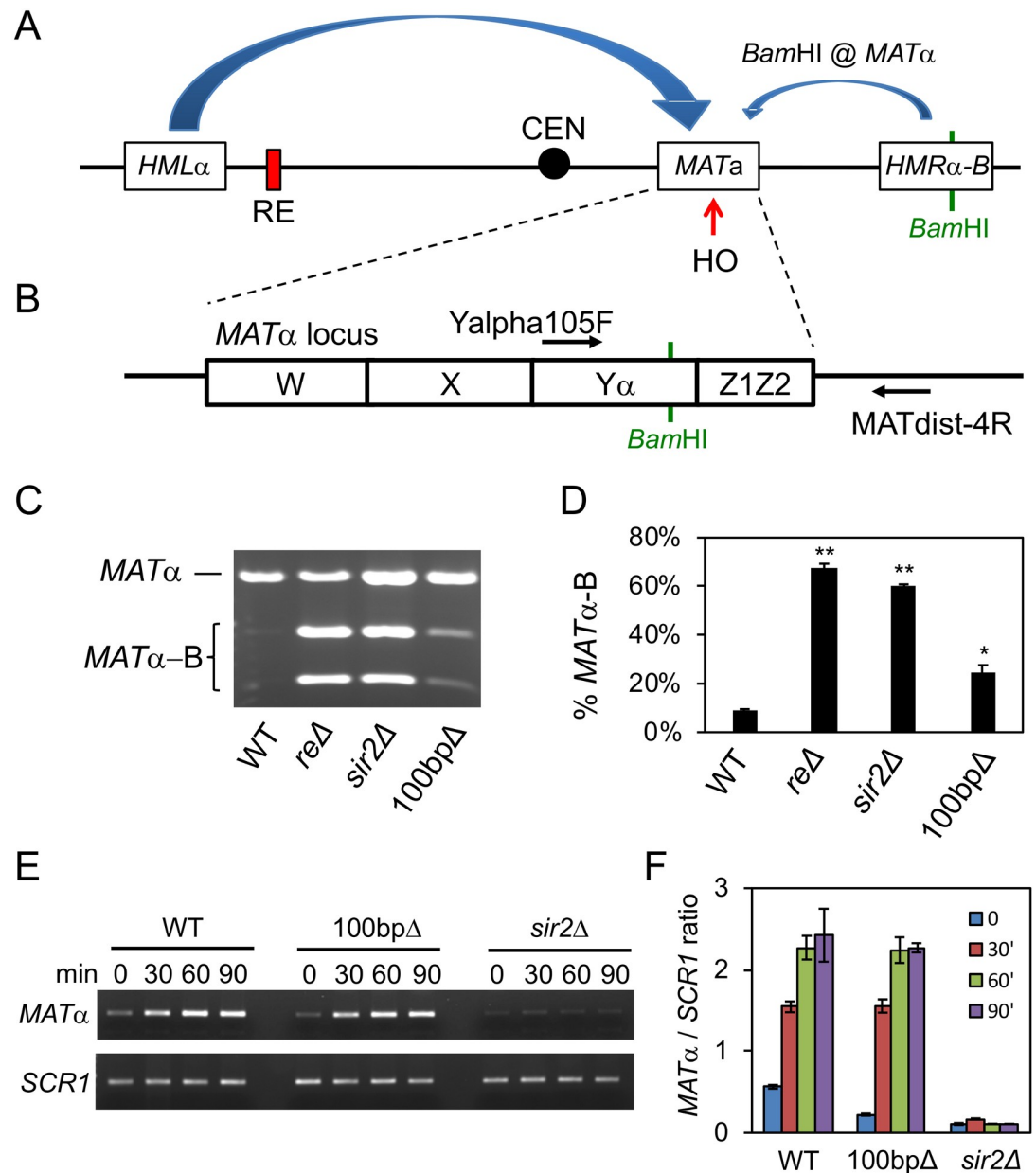


Fig 6. Loss of Sir2 and the Sir2/condensin binding site alters mating-type switching. (A) Schematic of a donor preference assay in which utilization of an artificial *HMR α -B* cassette as the donor for switching introduces a unique *Bam*HI site to the *MAT* locus. (B) Locations of primers flanking the *Bam*HI site used for PCR detection of *MAT α* . (C) Representative ethidium bromide stained agarose gel of *Bam*HI-digested *MAT α* PCR products after mating-type switching in WT (XW652), *re Δ* (XW676), *sir2 Δ* (ML557), and 100bp Δ (SY742) strains. The *MAT α -B* product is digested into 2 smaller bands. (D) Quantifying the percentage of *MAT α -B* PCR product digested by *Bam*HI, from three biological replicates. ImageJ was used for the quantitation. (**p* < 0.05, ***p* < 0.005). (E) Representative time course of switching from *MAT α* to *MAT α* in WT (ML447), 100bp Δ (ML460), and *sir2 Δ* (ML458) strains after HO was induced for 45 min and then shut down with glucose. Aliquots were harvested at 30 min intervals. *SCR1* is a control for input genomic DNA. (F) ImageJ quantification of *MAT α* PCR relative to *SCR1* for each time point. *n* = 3 biological replicates.

<https://doi.org/10.1371/journal.pgen.1008339.g006>

locus (reviewed in [5]). In this study we describe a previously unidentified Sir2 binding site that overlaps with a major non-rDNA condensin binding site within the RE on chromosome III in *MAT α* cells. Here, Sir2 regulates a small gene of unknown function called *RDT1*, which is transcriptionally activated during mating-type switching due to loss of repressive Sir2 from

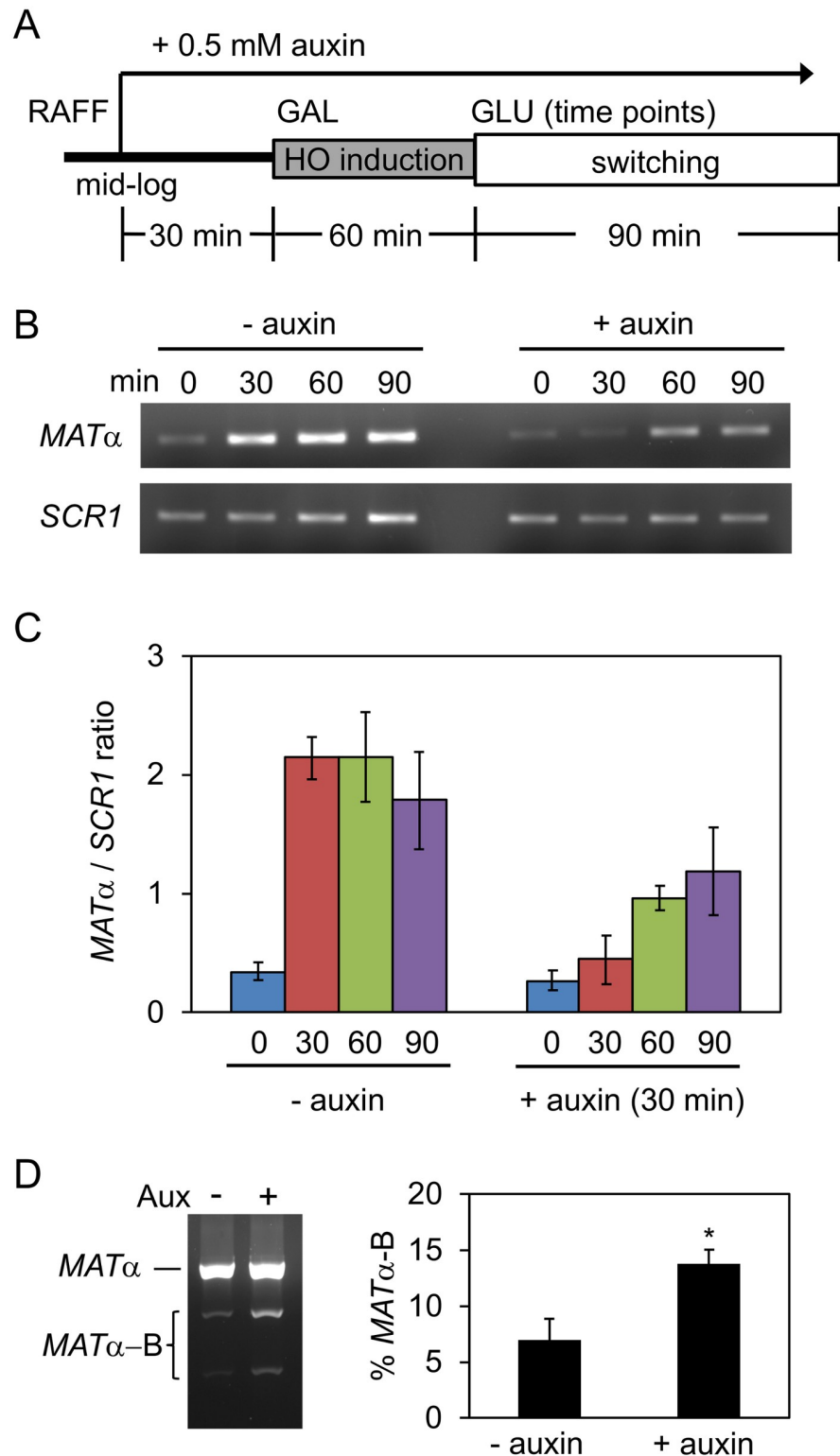


Fig 7. Effects of condensin depletion on mating-type switching. (A) Schematic of the time course used to deplete Brn1-AID prior to induction of mating-type switching in the ML1 strain background. Auxin was added 30 min prior to the induction of HO expression by galactose. (B) Representative EtBr stained agarose gel of *MATα* PCR products amplified from each time point during mating-type switching. *SCR1* PCR was used as a control for input DNA. (C) Quantification of the *MATα*/*SCR1* PCR product ratio across the time course from 3 biological replicates. (D) Effect of Brn1-AID depletion on mating-type switching donor preference. A representative biological replicate is shown, along with percentage use of *HMRα-B* cassette as the donor template. (**p* < 0.05).

<https://doi.org/10.1371/journal.pgen.1008339.g007>

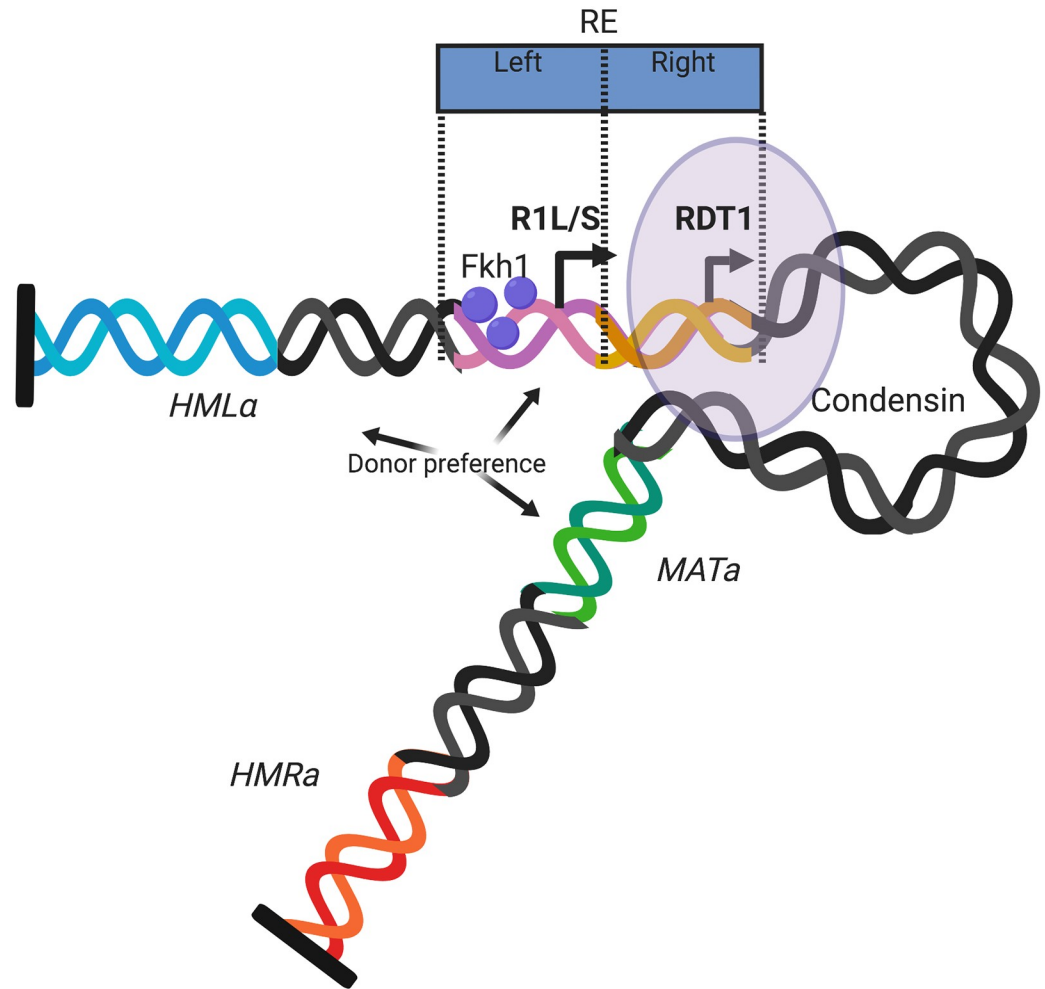


Fig 8. Model for cooperative regulation of chromosome III structure and donor preference by the bipartite RE. The left half of the RE regulates donor preference through expression of the R1L and R1S long ncRNAs and an array of Fkh1 proteins that interact with threonine-phosphorylated proteins at the double stranded DNA break at *MATa*. The right half of the RE is bound by condensin and Sir2. Like R1L/S, the expression of *RDT1* correlates with mating-type switching. Condensin is hypothesized to organize chromosome III structure through a unidirectional loop extrusion process that eventually places *MATa* into a chromosome-sized loop that helps insulates it from *HML* and *HMR* until condensin is removed at the time of switching. The loop is also likely maintained by clustering of telomeres and subtelomeres (black bars) and the heterochromatin set up by *HML* and *HMR*.

<https://doi.org/10.1371/journal.pgen.1008339.g008>

the *RDT1* promoter that correlates with binding to the HO-induced DSB at *MATa*. The *RDT1* RNA transcript is also translated into a small protein, but we have not yet been able to assign a function to the gene or protein because deleting the 28 amino acid ORF does not measurably alter mating-type switching when using *GAL-HO* based assays. It remains possible that deleting *RDT1* would have a significant effect on switching in the context of native HO expression, which is expressed only in mother cells during late G1, whereas the *GAL1-HO* is overexpressed in all cells throughout the cell cycle. Furthermore, *RDT1* and the R1L/S ncRNAs are themselves cell cycle regulated, similarly showing peak expression around late G1 [27]. Therefore, even with the Gal-HO induced system, the strong *RDT1* expression observed during switching (Fig 4D) suggests significant enrichment of G1 cells in the population. It is also possible that *RDT1* functions as a non-coding RNA that happens to be translated into a small non-functional peptide. Alternatively, transcription of *RDT1* could directly function in chromosome III

conformation by altering local chromatin accessibility at the promoter. Such a model was proposed for regulation of donor preference by transcription of the R1S/R1L non-coding RNAs [13, 27]. Dissecting the function(s) of *RDT1* through the cell cycle therefore remains an area of active investigation for the lab, and perhaps the key to fully understanding how its promoter functions as an LCR.

Functional complexity within the RE

While we do not yet know the molecular function of *RDT1* in mating-type regulation or other cellular processes, the promoter region of this gene clearly controls the structure of chromosome III. Three-dimensional chromatin structure has long been proposed to influence donor preference [40, 41]. However, deleting the minimal 700bp (left half) of the RE alters donor preference without a large change in chromosome III conformation. Furthermore, deleting the right half of the RE, which includes *RDT1*, changes chromosome III conformation without a dramatic change in donor preference [10, 13, 42]. Based on these findings it was proposed that the RE is a bipartite regulatory element [42], with the left half primarily responsible for donor preference activity and the right half for chromosome III structure. Our results support this view and narrow down the structural regulatory domain of the RE to a small (100bp) region of the *RDT1* promoter bound by the SIR and condensin complexes. Importantly, deleting this small region not only altered chromosome III structure, but also had a significant effect on donor preference, though not as strong as the *sir2Δ* mutation.

The coordination of *RDT1* expression with loss of Sir2/condensin binding at its promoter during mating-type switching, together with the loss of *HML-HMR* interaction in the 100bpΔ mutant, makes this site intriguingly similar to classic locus control regions (LCRs) in metazoans, which are cis-acting domains that contain a mixture of enhancers, insulators, chromatin opening elements, and tissue-specificity elements [33]. The minimal RE was previously described as an LCR in the context of donor preference [10], and transcription of the R1S/R1L long non-coding RNAs via activation by the 1st Mcm1/α2 binding site (DPS1) appears to be important for this activity in *MATa* cells [27]. We find that Sir2 indirectly supports donor preference from the left half of the RE in *MATa* cells by silencing *HMLALPHA2* expression, which prevents transcriptional repression by an Mcm1/α2 heterodimer, and by protecting the *HML* template from HO cleavage. Similarly, the loss of Sir2 also represses *RDT1* expression and condensin recruitment in the right half of the RE due to *HMLALPHA2* expression. It remains possible that SIR-dependent heterochromatin formation also directly contributes to the *HML-HMR* interaction through clustering. More clearly, however, Sir2 directly represses *RDT1* through localized histone deacetylation. How the loss of *RDT1* regulation and condensin recruitment changes chromosome III structure in the *sir2Δ* mutant remains unknown, but we propose that the *HMR-MATa* interaction is a default state, while the *HML-HMR* association has to be actively maintained by condensin and likely additional factors co-localized to this element, as well as SIR-dependent heterochromatin.

Interestingly, there also appears to be a functional relationship between the RE and silencing at the *HML* locus, such that deleting the left half of the RE specifically stabilizes *HML* silencing in *MATa* cells [43]. The mechanism involved remains unknown, but we hypothesize that eliminating this part of the RE could potentially allow the SIR and condensin complexes bound at the *RDT1* promoter to encroach and somehow enhance the heterochromatic structure at *HML*. Under this scenario, the left half of the RE could be insulating *HML* from the chromosomal organizing activity that occurs at the *RDT1* promoter.

Condensin function in mating-type switching

The *RDT1* promoter is a major condensin binding site identified by ChIP-seq (Fig 1), and given the strong Hi-C interaction between *HML* and *HMR*, we initially hypothesized that condensin at the *RDT1* promoter would crosslink with another condensin site bound on the right arm of chromosome III. However, this turned out to be unlikely because ChIP-seq of Smc4-myc did not reveal any strong peaks near *HMR*. The *S. cerevisiae* condensin complex was recently shown to catalyze ATP-dependent unidirectional loop extrusion using an *in vitro* single molecule assay [44]. The mechanism involves direct binding of condensin to DNA, followed by one end of the bound DNA being pulled inward as an extruded loop. Applying this model to the strong binding site at the *RDT1* promoter, this region could act as an anchor bound by condensin, with DNA to the right being rapidly extruded as a loop until pausing at *CEN3*. Extrusion would then continue at a slower rate toward *HMR*, allowing *HML* time to sample the entire right arm of chromosome III, until clustering with *HMR* (Fig 8). HOMER analysis of the Hi-C data in Fig 5B provides evidence for such a model because there is an ascending gradient of *HML* interaction frequency with sequences extending from the centromere region (bin 12) toward *HMR*, suggesting that *HML* “samples” the right arm of chromosome III. Once brought in contact, *HML* and *HMR* would then remain associated due to their heterochromatic states and shared retention at the nuclear envelope [45]. Formation of this loop appears to limit *HMR* association with *MATa*, but since the 100bp Δ mutation has no effect on the timing of switching, we do not believe that condensin at the *RDT1* promoter functions directly in the homologous recombination process. Rather, general Brn1 subunit depletion could slow the switching process by affecting chromosome III flexibility or conformational dynamics.

MATa specific recruitment of Sir2 and condensin to the RE

Condensin, and Sir2 each strongly associated with the *RDT1* promoter exclusively in *MATa* cells, though it is not clear if they bind at the same time, or are differentially bound throughout the cell cycle. Since DPS2 was required for Sir2 and condensin recruitment, and derepression of *HMLALPHA2* from *HML* also eliminated binding, we hypothesized and then demonstrated (S3 Fig) that Mcm1 was a key DNA binding factor involved. Mcm1 is a prototypical MADS box combinatorial transcription factor that derives its regulatory specificity through interactions with other factors, such as Ste12 in the case of *MATa* haploid-specific gene activation, or $\alpha 2$ when repressing the same target genes in *MAT α* cells [46]. This raises the question of whether Mcm1 directly recruits the SIR and condensin complexes, or perhaps additional factors that work with Mcm1 are involved. The latter is likely true because condensin and Sir2 are not recruited to the leftmost Mcm1/ $\alpha 2$ binding site in the left half of the RE, as indicated by the ChIP-seq data in Fig 1A. At the *RDT1* promoter, specificity for Sir2/condensin recruitment could originate from sequences underlying the condensin/Sir2 peaks. There are no traditional silencer-like sequences for SIR recruitment within the deleted 100bp (coordinates 30702 to 30801), and yeast condensin does not appear to have a consensus DNA binding sequence [47]. Closer inspection of the *RDT1* promoter indicates an A/T rich region with consensus binding sites for the transcription factors Fkh1/2 and Ash1, each of which regulates mating-type switching [11, 48, 49]. Fkh1 and Fkh2 also physically associate with Sir2 at the mitotic cyclin *CLB2* promoter during stress [50]. Ash1 is intriguing because it represses HO transcription in daughter cells [49, 51], raising the possibility of *RDT1* repression in daughter cells. Mcm1 activity in *MATa* cells could also indirectly establish a chromatin environment that is competent for Sir2/condensin recruitment, rather than direct recruitment through protein-protein interactions. In *MATa* cells, Mcm1 appears to prevent the strong nucleosome positioning

across the RE that occurs in *MAT α* cells [27], and indicative of an actively remodeled chromatin environment. Perhaps condensin is attracted to such regions, which is consistent with the association of condensin with promoters of active genes in mitotic cells, where enrichment was greatest at unwound regions of DNA [52]. Furthermore, nucleosome eviction by transcriptional coactivators was found to assist condensin loading in yeast [53], though the mechanism of loading remains poorly understood. Recruitment of condensin to the *RDT1* promoter LCR therefore provides an outstanding opportunity for dissecting mechanisms of condensin loading and function.

Methods

Yeast strains, plasmids, and media

Yeast strains were grown at 30°C in YPD or synthetic complete (SC) medium where indicated. The *SIR2*, or *HST1* open reading frames (ORFs) were deleted with *kanMX4* using one-step PCR-mediated gene replacement. *HML* was deleted and replaced with *LEU2*. Precise deletions of the 100bp condensin/Sir2 binding site within the *RDT1* promoter (chrIII coordinates 30701–30800), *DPS2* (chrIII coordinates 30557–30626), or the *RDT1* ORF (chrIII coordinates 30910–30996) were generated using the *delitto perfetto* method [32]. Endogenous *SIR2*, *BRN1*, or *SMC4* genes were C-terminally tagged with the 13xMyc epitope (13-EQKLISEEDL). Deletion and tagged gene combinations were generated through genetic crosses and tetrad dissection, including *Brn1* tagged with a V5-AID tag (template plasmids kindly provided by Vincent Guacci). All genetic manipulations were confirmed by PCR, and expression of tagged proteins confirmed by western blotting. The pGAL-HO-URA3 expression plasmid was kindly provided by Jessica Tyler [30]. Strain genotypes are provided in [S2 Table](#) and oligonucleotides listed in [S3 Table](#).

ChIP-seq analysis

Sir2 ChIP-seq was previously described [19]. For other ChIP-seq datasets, log-phase YPD cultures were cross-linked with 1% formaldehyde for 20 min, pelleted, washed with Tris-buffered saline (TBS), and then lysed in 600 μ l FA140 lysis buffer with glass beads using a mini-bead-beater (BioSpec Products). Lysates were removed from the beads and sonicated for 60 cycles (30s “on” and 30s “off” per cycle) in a Diagenode Bioruptor. Sonicated lysates were pelleted for 5 min at 14000 rpm in a microcentrifuge and the entire supernatant was transferred to a new microfuge tube and incubated overnight at 4°C with 5 μ g of anti-Myc antibody (9E10) and 20 μ l of protein G magnetic beads (Millipore). Following IP, the beads were washed once with FA140 buffer, twice with FA500 buffer, and twice with LiCl wash buffer. DNA was eluted from the beads in 1% SDS/TE buffer and cross-links were reversed overnight at 65°C. The chromatin was then purified using a Qiagen PCR purification kit. Libraries were constructed using the Illumina Truseq ChIP Sample Prep kit and TrueSeq standard protocol with 10ng of initial ChIP or Input DNA. Libraries that passed QC on a Bioanalyzer High Sensitivity DNA Chip (Agilent Technologies) were sequenced on an Illumina Miseq (UVA Genomic Analysis and Technology Core).

ChIP-seq computational analysis

Biological duplicate fastq files were concatenated together and reads mapped to the *sacCer3* genome using Bowtie with the following options:—best,—stratum,—nomaqround, and—m10 [54]. The resulting bam files were then converted into bigwig files using BEDTools [55]. As part of the pipeline, chromosome names were changed from the *sacCer3* NCBI values to values

readable by genomics viewers e.g. "ref[NC_001133]" to "chrI". The raw and processed datasets used in this study have been deposited in NCBI's GEO and are accessible through the GEO series accession number GSE92717. Downstream GO analysis was performed as follows. MACS2 was used to call peaks with the following options:—broad,—keep-dup, -tz 150, and -m 3, 1000 [56]. GFP peaks in the WT or *sir2Δ* backgrounds were subtracted from the WT *SMC4-13xMyc* and *sir2Δ SMC4-13xMyc* peaks, respectively, using BEDTools "intersect" with the -v option. The resulting normalized peaks were annotated using BEDTools "closest" with the -t all option specified, and in combination with a yeast gene list produced from USCS genome tables. The annotated peaks were then analyzed for GO terms using YeastMine (yeastmine.yeastgenome.org).

Hi-C analysis

Log-phase cultures were cross-linked with 3% formaldehyde for 20 min and quenched with a 2x volume of 2.5M Glycine. Cell pellets were washed with dH₂O and stored at -80°C. Thawed cells were resuspended in 5 ml of 1X NEB2 restriction enzyme buffer (New England Biolabs) and poured into a pre-chilled mortar containing liquid N₂. Nitrogen grinding was performed twice as previously described [57], and the lysates were then diluted to an OD₆₀₀ of 12 in 1x NEB2 buffer. 500 μl of cell lysate was used for each Hi-C library as follows. Lysates were solubilized by the addition of 50 μl 1% SDS and incubation at 65°C for 10 min. 55 μl of 10% TritonX-100 was added to quench the SDS, followed by 10 μl of 10X NEB2 buffer and 15 μl of *Hind*III (New England Biolabs, 20 U/μl) to digest at 37°C for 2 hr. An additional 10 μl of *Hind*III was added for digestion overnight. The remainder of the protocol was based on previously published work with minor exceptions [58]. In short, digested chromatin ends were filled-in with Klenow fragment (New England Biolabs) and biotinylated dCTP at 37°C for 1 hr, then heat inactivated at 70°C for 10 min. Ligation reactions with T4 DNA ligase were performed at 16°C for a minimum of 6 hr using the entire Hi-C sample diluted into a total volume of 4 ml. Proteinase K was added and cross-links were reversed overnight at 70°C. The ligated chromatin was phenol:chloroform extracted, ethanol precipitated, then resuspended in 500 μl dH₂O and treated with RNase A for 45 min. Following treatment with T4 DNA polymerase to remove biotinylated DNA ends that were unligated, the samples were concentrated with a Clean and Concentrator spin column (Zymogen, D4013) and sheared to approximately 300bp with a Diagenode Bioruptor. Biotinylated fragments were captured with 30 μl pre-washed Streptavidin Dynabeads (Invitrogen), then used for library preparation. Hi-C sequencing libraries were prepared with reagents from an Illumina Nextera Mate Pair Kit (FC-132-1001) using the standard Illumina protocol of End Repair, A-tailing, Adapter Ligation, and 12 cycles of PCR. PCR products were size selected and purified with AMPure XP beads before sequencing with an Illumina Miseq (UVA Genomic Analysis and Technology Core) or Hiseq (HudsonAlpha Institute for Biotechnology, Birmingham, AL). Raw and mapped reads are deposited at GEO (GSE92717).

Hi-C computational analysis

Iteratively corrected heatmaps were produced using python scripts from the Mirny lab hiclib library, <http://mirnylab.bitbucket.org/hiclib/index.html>. Briefly, reads were mapped using the iterative mapping program, which uses Bowtie2 to map reads and iteratively trims unmapped reads to increase the total number of mapped reads. Mapped reads were then parsed into an hdf5 python data dictionary for storage and further analysis. Mapped reads of the same strains were concatenated using the hiclib library's "Merge" function. Both individual and concatenated mapped reads have been deposited in GEO. Mapped reads were then run

through the fragment filtering program using the default parameters as follows: filterRsiteStart (offset = 5), filterDuplications, filterLarge, filterExtreme (cutH = 0.005, cutL = 0). Raw heat maps were further filtered to remove diagonal reads and iteratively corrected using the 03 heat map processing program. Finally, the iteratively corrected heatmaps were normalized for read count differences by dividing the sum of each row by the sum of the max row for a given plot, which drives all values towards 1 to make individual heatmaps comparable.

Observed/Expected heatmaps were created using HOMER Hi-C analysis software on the BAM file outputs from the iterativemapping program of the hiclib library python package [35]. Tag directories were created using all experimental replicates of a given biological sample and the `tbp -1` and `illuminaPE` options. Homer was also used to score differential chromosome interactions between the WT and mutant Hi-C heatmaps. The resulting list of differential interactions was uploaded into R where the given p-value was adjusted to a qvalue with `p.adjust`. An FDR cutoff of 0.05 was used to create a histogram of significantly different chromosome interactions in the mutants compared to WT. The histogram was further normalized by dividing the total number of significant differential interactions for a chromosome by total number of interactions called in the WT sample for that chromosome to account for size differences in the chromosomes. Thus, frequency represents the number of interactions that changed out of all possible interactions that could have changed.

RNA-seq data analysis

RNA-Seq data was acquired from GEO accessions GSE73274 [59] and GSE58319 [60] for the BY4742 (*MAT α*) and BY4741 (*MAT a*) backgrounds, respectively. Reads were then mapped to the *sacCer3* genome using Bowtie2 with no further processing of the resulting BAM files visualized in this paper.

3C assays

Chromosome Conformation Capture (3C) was performed in a similar manner to Hi-C with a few exceptions due to assay-specific quantification via quantitative real-time PCR rather than sequencing. Most notably, digested DNA ends were not filled in with dCTP-biotin before ligation and an un-crosslinked control library was created for each 3C library. Furthermore, all PCR reactions were normalized for starting DNA concentration using a *PDC1* intergenic region that is not recognized by *HindIII*, in addition to PCR of the un-crosslinked control for all tested looping interaction primer pairs.

Quantitative reverse transcriptase (RT) PCR assay

Total RNA (1 μ g) was used for cDNA synthesis with oligo(dT) and Superscript II reverse transcriptase as previously described [61]. Expression levels are indicated in figures relative to the level of *ACT1* mRNA, with this ratio then normalized to 1.0 for a specific strain or condition indicated for each experiment.

Western blots

Proteins were blotted using standard TCA extraction followed by SDS-PAGE as previously described [19]. Myc-tagged proteins were incubated with an anti-Myc primary antibody 9E10 (Millipore) at a 1:2000 dilution while tubulin was incubated with anti-Tubulin antibody B-5-1-2 (Sigma-Aldrich) at a 1:1500 dilution. The V5-AID tagged Brn1 was detected with anti-V5 antibody (Invitrogen, R96025) at a 1:4000 dilution. Primary antibodies were detected with an anti-mouse secondary antibody conjugated to HRP (Promega) at 1:5000 dilution in 5% fat-

free milk. Bands were then visualized with HyGlo (Denville Scientific) capture on autoradiography film (Denville Scientific).

Mating-type switching assays

For tracking the efficiency of switching, strains were transformed with pGAL-HO-*URA3*, pre-cultured in SC-ura + raffinose (2%) medium overnight, re-inoculated into the same medium ($OD_{600} = 0.05$) and then grown into log phase. Galactose (2%) was added to induce HO expression for 45 min. Glucose (2%) was then added and aliquots of the cultures were harvested at indicated time points. Genomic DNA was isolated and 10 ng used for PCR amplification. *MAT α* was detected using primers JS301 and JS302. The *SCR1* gene on chromosome V was used as a loading control (primers JS2665 and JS2666). PCR products were separated on a 1% agarose gel stained with ethidium bromide and then quantified using ImageJ. Donor preference with strains containing *HMR α -B* was performed as previously described [15]. Briefly, *MAT α* was amplified with primers Yalpha105F and MATdist-4R from genomic DNA 90 after switching was completed (90 min), and then digested with *Bam*HI. Ethidium stained bands were quantified using ImageJ. For the conditional V5-AID degenon strains, degradation of V5-AID-fused Brn1 protein was induced by addition of 0.5 mM indole-3-acetic acid (Auxin, Sigma # 13750).

For assaying HO cleavage across *MAT α* , *HML*, and *HMR*, the WT and *sir2 Δ* strains containing the pGAL-HO-*URA3* plasmid were induced with galactose for 0 to 2 hrs following growth in raffinose. Genomic DNA was then isolated and PCR across the HO-cleavage site performed with primers specific to each locus, and *SCR1* used as a loading control. *MAT α* was detected with JS301 and JS854, *HML* with JS3101 and JS3103, and *HMR* with JS3097 and JS3100. PCR was performed in the linear range and bands on ethidium stained agarose gels quantified with ImageJ. Real-time qPCR of *HML* and *HMR* with the same genomic DNA was performed with primers JS3101-JS3103, and JS3097-JS3098, respectively.

Supporting information

S1 Fig. *MAT α* -specific transcription of *RDT1* is repressed by Sir2 and Hst1. (A) IGV screenshot of compiled raw RNA-seq read data from BY4741 (*MAT α*) and BY4742 (*MAT α*) strains. The top two blue peaks represent Smc4-myc and Sir2-myc ChIP-seq reads. (B) Quantitative ChIP assay showing additional SIR complex subunit enrichment at the *RDT1* promoter. Signals are relative to input. (C) RT-qPCR showing effects of deleting *SIR2* and/or *HST1* on *RDT1* expression (relative to *ACT1*) when *HML* is present or deleted (* $p < 0.05$, ** $p < .005$). The WT *RDT1/ACT1* ratio is normalized to 1. (TIF)

S2 Fig. Deletion of Sir2 or the *RDT1* promoter Sir2/condensin binding site does not affect protein levels of Sir2 or Myc-tagged condensin subunits. (A) Western blot showing steady state Sir2 protein levels in WT (ML1), *sir2 Δ* (ML25), and 100bp Δ (ML275) strains. (B) Western blot with anti-Myc detection of Brn1-13xMyc or Sir2 in WT (ML149), *sir2 Δ* (ML161), and 100bp Δ (ML322) strains. (C) Western blot with anti-Myc detection of Smc4-13xMyc or Sir2 in WT (ML152), *sir2 Δ* (ML160), and 100bp Δ version. (TIF)

S3 Fig. The *RDT1*-proximal Mcm1/ α 2 binding site (DPS2) is important for Sir2 and condensin recruitment. (A) Schematic diagram depicting the location of the DPS2 sequence deletion relative to other elements with the RE, with the deleted chromosome III coordinates indicated in red. (B) Quantitative ChIP of native Sir2 in WT and *dps2 Δ* strains. (C) Quantitative

ChIP of Brn1-Myc in WT and *dps2Δ* strains. @*RDT1* promoter indicates enrichment at the Sir2/condensin peak. ChIP signals are plotted relative to the input signal. (** $p < 0.005$). (TIF)

S4 Fig. Deletion of the *RDT1* open reading frame has no effect on mating-type switching. (A) Representative time course of switching from *MATa* to *MATα* in WT (ML440) and *rdt1Δ* (ML443) strains. PCR products are specific to *MATα* and an *SCR1* loading control. (B) Quantitation of the average *MATα/SCR1* PCR signal ratio from 3 biological replicates. (C) Schematic of chromosome III in the donor preference reporter strain harboring an artificial *HMRα*-B cassette as the donor for switching, which introduces a unique *Bam*HI site to the *MAT* locus. (D) Representative ethidium bromide stained agarose gel of *Bam*HI-digested *MATα* PCR products after mating-type switching in WT (XW652) and *rdt1Δ* (MD30) strains. The bottom two bands represent *HMR*-derived switching. (E) Quantitation of average *MATα*-B utilization from 3 biological replicates. (TIF)

S5 Fig. Deleting the Sir2/condensin binding site within the RE (100bpΔ) does not alter Sir2 function at *HMLα*. (A) Quantitative mating assay for WT (ML1) and 100bpΔ (ML275) strains. (B) Quantitative ChIP assay showing Sir2 enrichment at *HML-I* in WT (ML1) and 100bpΔ (ML275) strains. (** $p < 0.005$). (TIF)

S6 Fig. *HML* is accessible to cleavage by HO endonuclease in *sir2Δ* strains. (A) PCR amplification of *MATa*, *HML*, *HMR*, and *SCR1* loci from *MATa* WT (ML440) and *sir2Δ* (MD29) strains containing the pGAL-HO-URA3 expression vector. Times after HO induction with galactose are indicated. A representative experiment is depicted. (B) Quantitation of mean *MATa* PCR signal, relative to the *SCR1* control, from 3 independent biological replicates. Error bars indicate standard deviation. (C) Quantitation of mean *HML* PCR signal, as done for panel B. (D) Quantitation of mean *HMR* PCR signal, as done for panel B. (E and F) Real-time qPCR signal, relative to *SCR1* control, for *HML* and *HMR*, respectively. The PCR signal at time 0 is normalized to 1.0 in each panel. (TIF)

S7 Fig. Auxin inducible degron (AID)-mediated depletion of Brn1 does not derepress *RDT1* or *HMLα*. (A) Western blot time course of auxin induced degradation of Brn1-V5. Time indicates minutes after addition of auxin. (B) ChIP assay showing Brn1-V5 enrichment at the *RDT1* promoter with and without auxin addition. The Brn1-V5 signal is relative to input and the ratio from an untagged control strain is normalized to 1. (C) RT-qPCR of *RDT1* expression following 30 or 60 minutes of Brn1 depletion by auxin. (D) RT-qPCR of *HMLAL-PHA2* expression following 30 or 60 min of Brn1 depletion by auxin. In panels C and D, the signals are relative to *ACT1* control and normalized to 1.0 without auxin. (TIF)

S1 Table. Genes closest to Sir2-dependent condensin peaks. This Excel spreadsheet lists the systematic ORF names of all genes that were closest to Sir2-dependent condensin peaks, as chosen using MACS. (XLSX)

S2 Table. Yeast strains. List of all *Saccharomyces cerevisiae* strains used in this study, along with their genotypes and source. (DOCX)

S3 Table. Oligonucleotides. List of oligodeoxynucleotides used in this study. (DOCX)

Acknowledgments

We thank Job Dekker, Jon Belton, Maitreya Dunham, Ivan Liachko, Maxim Imakev, and Anton Goloborodko for advice on Hi-C protocols and analysis methods. We also thank James Haber, Andrew Murray, Jasper Rine, Jessica Tyler, Alan Hinnebusch, Marc Gartenberg, Dan Gottschling, and Vincent Guacci for kindly providing yeast strains, plasmids, or antibodies. We thank David Auble and Patrick Grant for critically reading the manuscript and providing suggestions prior to submission, and Elisa Enriquez Hesles for Fig 8 artwork.

Author Contributions

Conceptualization: Mingguang Li, Ryan D. Fine, Jeffrey S. Smith.

Data curation: Ryan D. Fine.

Formal analysis: Jeffrey S. Smith.

Funding acquisition: Jeffrey S. Smith.

Investigation: Mingguang Li, Ryan D. Fine, Manikarna Dinda.

Methodology: Mingguang Li, Ryan D. Fine, Manikarna Dinda, Stefan Bekiranov.

Project administration: Jeffrey S. Smith.

Software: Ryan D. Fine.

Supervision: Stefan Bekiranov, Jeffrey S. Smith.

Validation: Manikarna Dinda.

Visualization: Ryan D. Fine.

Writing – original draft: Mingguang Li, Ryan D. Fine, Jeffrey S. Smith.

Writing – review & editing: Mingguang Li, Ryan D. Fine, Manikarna Dinda, Stefan Bekiranov, Jeffrey S. Smith.

References

1. Haber JE. Mating-type genes and *MAT* switching in *Saccharomyces cerevisiae*. *Genetics*. 2012; 191(1):33–64. <https://doi.org/10.1534/genetics.111.134577> PMID: 2255442.
2. Haber JE, George JP. A mutation that permits the expression of normally silent copies of mating-type information in *Saccharomyces cerevisiae*. *Genetics*. 1979; 93(1):13–35. PMID: 16118901.
3. Klar AJ, Fogel S, Macleod K. *MAR1*-a regulator of the *HMa* and *HMa* loci in *Saccharomyces cerevisiae*. *Genetics*. 1979; 93(1):37–50. PMID: 17248968.
4. Rine J. Regulation and Transposition of Cryptic Mating Type Genes in *Saccharomyces cerevisiae*. Eugene, OR: University of Oregon; 1979.
5. Gartenberg MR, Smith JS. The nuts and bolts of transcriptionally silent chromatin in *Saccharomyces cerevisiae*. *Genetics*. 2016; 203(4):1563–99. <https://doi.org/10.1534/genetics.112.145243> PMID: 27516616.
6. Strathern JN, Klar AJ, Hicks JB, Abraham JA, Ivy JM, Nasmyth KA, et al. Homothallic switching of yeast mating type cassettes is initiated by a double-stranded cut in the *MAT* locus. *Cell*. 1982; 31(1):183–92. [https://doi.org/10.1016/0092-8674\(82\)90418-4](https://doi.org/10.1016/0092-8674(82)90418-4) PMID: 6297747.
7. Haber JE, Rogers DT, McCusker JH. Homothallic conversions of yeast mating-type genes occur by intrachromosomal recombination. *Cell*. 1980; 22:277–89. [https://doi.org/10.1016/0092-8674\(80\)90175-0](https://doi.org/10.1016/0092-8674(80)90175-0) PMID: 6253081.

8. Nasmyth K. The determination of mother cell-specific mating type switching in yeast by a specific regulator of HO transcription. *EMBO J.* 1987; 6(1):243–8. PMID: [15981333](https://pubmed.ncbi.nlm.nih.gov/15981333/).
9. Klar AJ, Hicks JB, Strathern JN. Directionality of yeast mating-type interconversion. *Cell.* 1982; 28(3):551–61. [https://doi.org/10.1016/0092-8674\(82\)90210-0](https://doi.org/10.1016/0092-8674(82)90210-0) PMID: [7042099](https://pubmed.ncbi.nlm.nih.gov/7042099/).
10. Wu X, Haber JE. A 700 bp cis-acting region controls mating-type dependent recombination along the entire left arm of yeast chromosome III. *Cell.* 1996; 87(2):277–85. [https://doi.org/10.1016/s0092-8674\(00\)81345-8](https://doi.org/10.1016/s0092-8674(00)81345-8) PMID: [8861911](https://pubmed.ncbi.nlm.nih.gov/8861911/).
11. Sun K, Coic E, Zhou Z, Durrens P, Haber JE. *Saccharomyces* forkhead protein Fkh1 regulates donor preference during mating-type switching through the recombination enhancer. *Genes Dev.* 2002; 16(16):2085–96. <https://doi.org/10.1101/gad.994902> PMID: [12183363](https://pubmed.ncbi.nlm.nih.gov/12183363/).
12. Wu C, Weiss K, Yang C, Harris MA, Tye BK, Newlon CS, et al. Mcm1 regulates donor preference controlled by the recombination enhancer in *Saccharomyces* mating-type switching. *Genes Dev.* 1998; 12(11):1726–37. <https://doi.org/10.1101/gad.12.11.1726> PMID: [9620858](https://pubmed.ncbi.nlm.nih.gov/9620858/).
13. Szeto L, Fafalios MK, Zhong H, Vershon AK, Broach JR. α 2p controls donor preference during mating type interconversion in yeast by inactivating a recombinational enhancer of chromosome III. *Genes Dev.* 1997; 11(15):1899–911. <https://doi.org/10.1101/gad.11.15.1899> PMID: [9271114](https://pubmed.ncbi.nlm.nih.gov/9271114/).
14. Dummer AM, Su Z, Cherney R, Choi K, Denu J, Zhao X, et al. Binding of the Fkh1 Forkhead associated domain to a phosphopeptide within the Mph1 DNA helicase regulates mating-type switching in budding Yeast. *PLoS Genet.* 2016; 12(6):e1006094. <https://doi.org/10.1371/journal.pgen.1006094> PMID: [27257873](https://pubmed.ncbi.nlm.nih.gov/27257873/).
15. Li J, Coic E, Lee K, Lee CS, Kim JA, Wu Q, et al. Regulation of budding yeast mating-type switching donor preference by the FHA domain of Fkh1. *PLoS Genet.* 2012; 8(4):e1002630. <https://doi.org/10.1371/journal.pgen.1002630> PMID: [22496671](https://pubmed.ncbi.nlm.nih.gov/22496671/).
16. Jensen R, Sprague GF Jr., Herskowitz I. Regulation of yeast mating-type interconversion: feedback control of HO gene expression by the mating-type locus. *Proc Natl Acad Sci U S A.* 1983; 80(10):3035–9. <https://doi.org/10.1073/pnas.80.10.3035> PMID: [6344075](https://pubmed.ncbi.nlm.nih.gov/6344075/).
17. Klar AJ, Hicks JB, Strathern JN. Irregular transpositions of mating-type genes in yeast. *Cold Spring Harb Symp Quant Biol.* 1981; 45 Pt 2:983–90. <https://doi.org/10.1101/sqb.1981.045.01.114> PMID: [6266771](https://pubmed.ncbi.nlm.nih.gov/6266771/).
18. Nasmyth KA. The regulation of yeast mating-type chromatin structure by SIR: an action at a distance affecting both transcription and transposition. *Cell.* 1982; 30(2):567–78. [https://doi.org/10.1016/0092-8674\(82\)90253-7](https://doi.org/10.1016/0092-8674(82)90253-7) PMID: [6215985](https://pubmed.ncbi.nlm.nih.gov/6215985/).
19. Li M, Valsakumar V, Poorey K, Bekiranov S, Smith JS. Genome-wide analysis of functional sirtuin chromatin targets in yeast. *Genome Biol.* 2013; 14(5):R48. <https://doi.org/10.1186/gb-2013-14-5-r48> PMID: [23710766](https://pubmed.ncbi.nlm.nih.gov/23710766/).
20. D'Ambrosio C, Schmidt CK, Katou Y, Kelly G, Itoh T, Shirahige K, et al. Identification of cis-acting sites for condensin loading onto budding yeast chromosomes. *Genes Dev.* 2008; 22(16):2215–27. <https://doi.org/10.1101/gad.1675708> PMID: [18708580](https://pubmed.ncbi.nlm.nih.gov/18708580/).
21. Teytelman L, Thurtle DM, Rine J, van Oudenaarden A. Highly expressed loci are vulnerable to misleading ChIP localization of multiple unrelated proteins. *Proc Natl Acad Sci U S A.* 2013; 110(46):18602–7. <https://doi.org/10.1073/pnas.1316064110> PMID: [24173036](https://pubmed.ncbi.nlm.nih.gov/24173036/).
22. Bhalla N, Biggins S, Murray AW. Mutation of YCS4, a budding yeast condensin subunit, affects mitotic and nonmitotic chromosome behavior. *Mol Biol Cell.* 2002; 13(2):632–45. <https://doi.org/10.1091/mbc.01-05-0264> PMID: [11854418](https://pubmed.ncbi.nlm.nih.gov/11854418/).
23. Wilson BA, Masel J. Putatively noncoding transcripts show extensive association with ribosomes. *Genome Biol Evol.* 2011; 3:1245–52. <https://doi.org/10.1093/gbe/evr099> PMID: [21948395](https://pubmed.ncbi.nlm.nih.gov/21948395/).
24. Suka N, Suka Y, Carmen AA, Wu J, Grunstein M. Highly specific antibodies determine histone acetylation site usage in yeast heterochromatin and euchromatin. *Mol Cell.* 2001; 8(2):473–9. PMID: [11545749](https://pubmed.ncbi.nlm.nih.gov/11545749/).
25. Davie JK, Edmondson DG, Coco CB, Dent SY. Tup1-Ssn6 interacts with multiple class I histone deacetylases *in vivo*. *J Biol Chem.* 2003; 278(50):50158–62. <https://doi.org/10.1074/jbc.M309753200> PMID: [14525981](https://pubmed.ncbi.nlm.nih.gov/14525981/).
26. Wu J, Suka N, Carlson M, Grunstein M. TUP1 utilizes histone H3/H2B-specific HDA1 deacetylase to repress gene activity in yeast. *Mol Cell.* 2001; 7(1):117–26. PMID: [11172717](https://pubmed.ncbi.nlm.nih.gov/11172717/).
27. Ercan S, Reese JC, Workman JL, Simpson RT. Yeast recombination enhancer is stimulated by transcription activation. *Mol Cell Biol.* 2005; 25(18):7976–87. <https://doi.org/10.1128/MCB.25.18.7976-7987.2005> PMID: [16135790](https://pubmed.ncbi.nlm.nih.gov/16135790/).
28. Kressler D, Rojo M, Linder P, Cruz J. Spb1p is a putative methyltransferase required for 60S ribosomal subunit biogenesis in *Saccharomyces cerevisiae*. *Nucleic Acids Res.* 1999; 27(23):4598–608. <https://doi.org/10.1093/nar/27.23.4598> PMID: [10556316](https://pubmed.ncbi.nlm.nih.gov/10556316/).

29. Loo S, Laurenson P, Foss M, Dillin A, Rine J. Roles of *ABF1*, *NPL3*, and *YCL54* in silencing in *Saccharomyces cerevisiae*. *Genetics*. 1995; 141(3):889–902. PMID: [8582634](#).
30. Tamburini BA, Tyler JK. Localized histone acetylation and deacetylation triggered by the homologous recombination pathway of double-strand DNA repair. *Mol Cell Biol*. 2005; 25(12):4903–13. <https://doi.org/10.1128/MCB.25.12.4903-4913.2005> PMID: [15923609](#).
31. Mills KD, Sinclair DA, Guarente L. MEC1-dependent redistribution of the Sir3 silencing protein from telomeres to DNA double-strand breaks. *Cell*. 1999; 97(5):609–20. [https://doi.org/10.1016/s0092-8674\(00\)80772-2](https://doi.org/10.1016/s0092-8674(00)80772-2) PMID: [10367890](#).
32. Storici F, Lewis LK, Resnick MA. *In vivo* site-directed mutagenesis using oligonucleotides. *Nat Biotechnol*. 2001; 19(8):773–6. <https://doi.org/10.1038/90837> PMID: [11479573](#).
33. Li Q, Peterson KR, Fang X, Stamatoyannopoulos G. Locus control regions. *Blood*. 2002; 100(9):3077–86. <https://doi.org/10.1182/blood-2002-04-1104> PMID: [12384402](#).
34. Tsai YC, Cooke NE, Liebhaber SA. Long-range looping of a locus control region drives tissue-specific chromatin packing within a multigene cluster. *Nucleic Acids Res*. 2016; 44(10):4651–64. <https://doi.org/10.1093/nar/gkw090> PMID: [26893355](#).
35. Heinz S, Benner C, Spann N, Bertolino E, Lin YC, Laslo P, et al. Simple combinations of lineage-determining transcription factors prime cis-regulatory elements required for macrophage and B cell identities. *Mol Cell*. 2010; 38(4):576–89. <https://doi.org/10.1016/j.molcel.2010.05.004> PMID: [20513432](#).
36. Miele A, Bystricky K, Dekker J. Yeast silent mating type loci form heterochromatic clusters through silencer protein-dependent long-range interactions. *PLoS Genet*. 2009; 5(5):e1000478. <https://doi.org/10.1371/journal.pgen.1000478> PMID: [19424429](#).
37. Imakaev M, Fudenberg G, McCord RP, Naumova N, Goloborodko A, Lajoie BR, et al. Iterative correction of Hi-C data reveals hallmarks of chromosome organization. *Nat Methods*. 2012; 9(10):999–1003. <https://doi.org/10.1038/nmeth.2148> PMID: [22941365](#).
38. Miyazaki T, Bressan DA, Shinohara M, Haber JE, Shinohara A. *In vivo* assembly and disassembly of Rad51 and Rad52 complexes during double-strand break repair. *EMBO J*. 2004; 23(4):939–49. <https://doi.org/10.1038/sj.emboj.7600091> PMID: [14765116](#).
39. Nishimura K, Fukagawa T, Takisawa H, Kakimoto T, Kanemaki M. An auxin-based degron system for the rapid depletion of proteins in nonplant cells. *Nat Methods*. 2009; 6(12):917–22. <https://doi.org/10.1038/nmeth.1401> PMID: [19915560](#).
40. Coic E, Richard GF, Haber JE. *Saccharomyces cerevisiae* donor preference during mating-type switching is dependent on chromosome architecture and organization. *Genetics*. 2006; 173(3):1197–206. <https://doi.org/10.1534/genetics.106.055392> PMID: [16624909](#).
41. Wu X, Haber JE. *MATa* donor preference in yeast mating-type switching: activation of a large chromosomal region for recombination. *Genes Dev*. 1995; 9(15):1922–32. <https://doi.org/10.1101/gad.9.15.1922> PMID: [7649475](#).
42. Belton JM, Lajoie BR, Audibert S, Cantaloube S, Lassadi I, Goiffon I, et al. The conformation of yeast chromosome III is mating type dependent and controlled by the recombination enhancer. *Cell Rep*. 2015; 13(9):1855–67. <https://doi.org/10.1016/j.celrep.2015.10.063> PMID: [26655901](#).
43. Dodson AE, Rine J. Donor preference meets heterochromatin: Moonlighting activities of a recombinational enhancer in *Saccharomyces cerevisiae*. *Genetics*. 2016; 204(1):177–90. PMID: [27489001](#).
44. Ganji M, Shaltiel IA, Bisht S, Kim E, Kalichava A, Haering CH, et al. Real-time imaging of DNA loop extrusion by condensin. *Science*. 2018; 360(6384):102–5. <https://doi.org/10.1126/science.aar7831> PMID: [29472443](#).
45. Bystricky K, Van Attikum H, Montiel MD, Dion V, Gehlen L, Gasser SM. Regulation of nuclear positioning and dynamics of the silent mating type loci by the yeast Ku70/Ku80 complex. *Mol Cell Biol*. 2009; 29(3):835–48. <https://doi.org/10.1128/MCB.01009-08> PMID: [19047366](#).
46. Messenguy F, Dubois E. Role of MADS box proteins and their cofactors in combinatorial control of gene expression and cell development. *Gene*. 2003; 316:1–21. [https://doi.org/10.1016/s0378-1119\(03\)00747-9](https://doi.org/10.1016/s0378-1119(03)00747-9) PMID: [14563547](#).
47. Wang BD, Eyre D, Basrai M, Lichten M, Strunnikov A. Condensin binding at distinct and specific chromosomal sites in the *Saccharomyces cerevisiae* genome. *Mol Cell Biol*. 2005; 25(16):7216–25. <https://doi.org/10.1128/MCB.25.16.7216-7225.2005> PMID: [16055730](#).
48. Bobola N, Jansen RP, Shin TH, Nasmyth K. Asymmetric accumulation of Ash1p in postanaphase nuclei depends on a myosin and restricts yeast mating-type switching to mother cells. *Cell*. 1996; 84(5):699–709. [https://doi.org/10.1016/s0092-8674\(00\)81048-x](https://doi.org/10.1016/s0092-8674(00)81048-x) PMID: [8625408](#).
49. Sil A, Herskowitz I. Identification of asymmetrically localized determinant, Ash1p, required for lineage-specific transcription of the yeast *HO* gene. *Cell*. 1996; 84(5):711–22. [https://doi.org/10.1016/s0092-8674\(00\)81049-1](https://doi.org/10.1016/s0092-8674(00)81049-1) PMID: [8625409](#).

50. Linke C, Klipp E, Lehrach H, Barberis M, Krobitsch S. Fkh1 and Fkh2 associate with Sir2 to control *CLB2* transcription under normal and oxidative stress conditions. *Front Physiol.* 2013; 4:173. <https://doi.org/10.3389/fphys.2013.00173> PMID: 23874301.
51. Long RM, Singer RH, Meng X, Gonzalez I, Nasmyth K, Jansen RP. Mating type switching in yeast controlled by asymmetric localization of *ASH1* mRNA. *Science.* 1997; 277(5324):383–7. <https://doi.org/10.1126/science.277.5324.383> PMID: 9219698.
52. Sutani T, Sakata T, Nakato R, Masuda K, Ishibashi M, Yamashita D, et al. Condensin targets and reduces unwound DNA structures associated with transcription in mitotic chromosome condensation. *Nat Commun.* 2015; 6:7815. <https://doi.org/10.1038/ncomms8815> PMID: 26204128.
53. Toselli-Mollereau E, Robellet X, Fauque L, Lemaire S, Schiklenk C, Klein C, et al. Nucleosome eviction in mitosis assists condensin loading and chromosome condensation. *EMBO J.* 2016; 35(14):1565–81. <https://doi.org/10.15252/emj.201592849> PMID: 27266525.
54. Langmead B, Trapnell C, Pop M, Salzberg SL. Ultrafast and memory-efficient alignment of short DNA sequences to the human genome. *Genome Biol.* 2009; 10(3):R25. <https://doi.org/10.1186/gb-2009-10-3-r25> PMID: 19261174.
55. Quinlan AR, Hall IM. BEDTools: a flexible suite of utilities for comparing genomic features. *Bioinformatics.* 2010; 26(6):841–2. <https://doi.org/10.1093/bioinformatics/btq033> PMID: 20110278.
56. Liu T. Use model-based Analysis of ChIP-Seq (MACS) to analyze short reads generated by sequencing protein-DNA interactions in embryonic stem cells. *Methods Mol Biol.* 2014; 1150:81–95. https://doi.org/10.1007/978-1-4939-0512-6_4 PMID: 24743991.
57. Belton JM, Dekker J. Measuring chromatin structure in budding yeast. *Cold Spring Harb Protoc.* 2015; 2015(7):614–8. <https://doi.org/10.1101/pdb.top077552> PMID: 26134912.
58. Burton JN, Liachko I, Dunham MJ, Shendure J. Species-level deconvolution of metagenome assemblies with Hi-C-based contact probability maps. *G3 (Bethesda).* 2014; 4(7):1339–46. <https://doi.org/10.1534/g3.114.011825> PMID: 24855317.
59. Porter DF, Koh YY, VanVeller B, Raines RT, Wickens M. Target selection by natural and redesigned PUF proteins. *Proc Natl Acad Sci U S A.* 2015; 112(52):15868–73. <https://doi.org/10.1073/pnas.1508501112> PMID: 26668354.
60. Swamy KB, Lin CH, Yen MR, Wang CY, Wang D. Examining the condition-specific antisense transcription in *S. cerevisiae* and *S. paradoxus*. *BMC Genomics.* 2014; 15:521. <https://doi.org/10.1186/1471-2164-15-521> PMID: 24965678.
61. Li M, Petteys BJ, McClure JM, Valsakumar V, Bekiranov S, Frank EL, et al. Thiamine biosynthesis in *Saccharomyces cerevisiae* is regulated by the NAD⁺-dependent histone deacetylase Hst1. *Mol Cell Biol.* 2010; 30(13):3329–41. <https://doi.org/10.1128/MCB.01590-09> PMID: 20439498.